

Tectonic evolution of the early Mesozoic blueschist-bearing Qiangtang metamorphic belt, central Tibet

Paul Kapp,¹ An Yin, Craig E. Manning, T. Mark Harrison,² and Michael H. Taylor

Department of Earth and Space Sciences and Institute of Geophysics and Planetary Physics, University of California, Los Angeles, California, USA

Lin Ding

Institute of Geology and Geophysics, Lithosphere Tectonic Evolution Lab, Chinese Academy of Sciences, Beijing, People's Republic of China

Received 11 March 2002; revised 22 December 2002; accepted 13 March 2003; published 28 August 2003.

[1] A >500-km-long east-west trending metamorphic belt in the Qiangtang terrane of central Tibet consists of tectonic melange that occurs in the footwalls of Late Triassic–Early Jurassic domal low-angle normal faults. The melange is comprised of a strongly deformed matrix of metasedimentary and mafic schists that encloses lesser-deformed blocks of metabasites, Carboniferous–Triassic metasedimentary rocks, and early Paleozoic gneiss. Both the blocks and melange matrix exhibit greenschist, epidote-blueschist, and locally, epidote-amphibolite facies mineral assemblages. Thermobarometry reveals that the metamorphic belt experienced pressures of >10 kbar. Maximum equilibration temperatures for mafic schists in the melange matrix decrease from east to west, from ~660°C near Shuang Hu (33°N, 89°E), ~500°C near Rongma (33°N, 87°E), to ~425°C near Gangma Co (34°N, 84°E). Equilibration at consistently high pressures over a large range of temperatures is compatible with metamorphism of Qiangtang melange within a low-angle subduction zone beneath a continental margin. Coupled structural, thermobarometric, and ⁴⁰Ar/³⁹Ar studies suggest that Qiangtang melange was exhumed in an intracontinental setting from depths of >35 km to upper crustal levels in <12 Myr by Late Triassic–Early Jurassic crustal-scale normal faulting. Detrital zircons from metasandstones within the melange matrix yield U-Pb ion-microprobe ages that range from early Paleozoic to Early Archean, and could have been sourced from terranes to the north of the Jinsha suture. Our results support a model in which Qiangtang melange was underthrust ~200 km beneath the Qiangtang terrane during early Mesozoic flat-slab

southward subduction of Paleo-Tethyan oceanic lithosphere along the Jinsha suture. This model predicts that significant portions of the central Tibetan continental mantle lithosphere were removed during early Mesozoic low-angle oceanic subduction and that the present-day central Tibetan deeper crust includes large volumes of underthrust early Mesozoic melange. **INDEX TERMS:** 8109 Tectonophysics: Continental tectonics—extensional (0905); 9320 Information Related to Geographic Region: Asia; 8015 Structural Geology: Local crustal structure; 1035 Geochemistry: Geochronology; 3660 Mineralogy and Petrology: Metamorphic petrology; **KEYWORDS:** Tibet, blueschist, melange, exhumation, subduction, metamorphic core complex. **Citation:** Kapp, P., A. Yin, C. E. Manning, T. M. Harrison, M. H. Taylor, and L. Ding, Tectonic evolution of the early Mesozoic blueschist-bearing Qiangtang metamorphic belt, central Tibet, *Tectonics*, 22(4), 1043, doi:10.1029/2002TC001383, 2003.

1. Introduction

[2] Knowledge of the pre-Cenozoic lithospheric architecture of Tibet is critical for providing initial conditions for models of Tibetan plateau formation, for establishing strain markers to quantify Cenozoic deformation, and for the development of hypotheses to explain heterogeneous tectonism related to the Cenozoic Indo-Asian collision. From north to south, Tibet is comprised of the Kunlun, Songpan-Ganzi flysch complex, Qiangtang, and Lhasa terranes, which are separated by ~east striking suture zones of late Paleozoic to Mesozoic age (Figure 1) [Chang and Zheng, 1973; Dewey and Burke, 1973; Allègre *et al.*, 1984; Dewey *et al.*, 1988; Yin and Harrison, 2000]. However, these terranes and suture zones have been studied only in reconnaissance fashion and are poorly characterized. This is especially true for central Tibet, where a >500-km-long and up to 100-km-wide blueschist-bearing metamorphic belt occurs within the central Qiangtang terrane (Figure 1) [Hennig, 1915; Cheng and Xu, 1986; Li *et al.*, 1995; Bao *et al.*, 1999; Kapp *et al.*, 2000].

[3] The central Qiangtang metamorphic belt (CQMB) was initially interpreted to be Paleozoic and older basement of the Qiangtang terrane, as it was mapped to be non-

¹Now at Department of Geosciences, University of Arizona, Tucson, Arizona, USA.

²Also at Institute of Advanced Studies, Australian National University, Canberra, ACT, Australia.

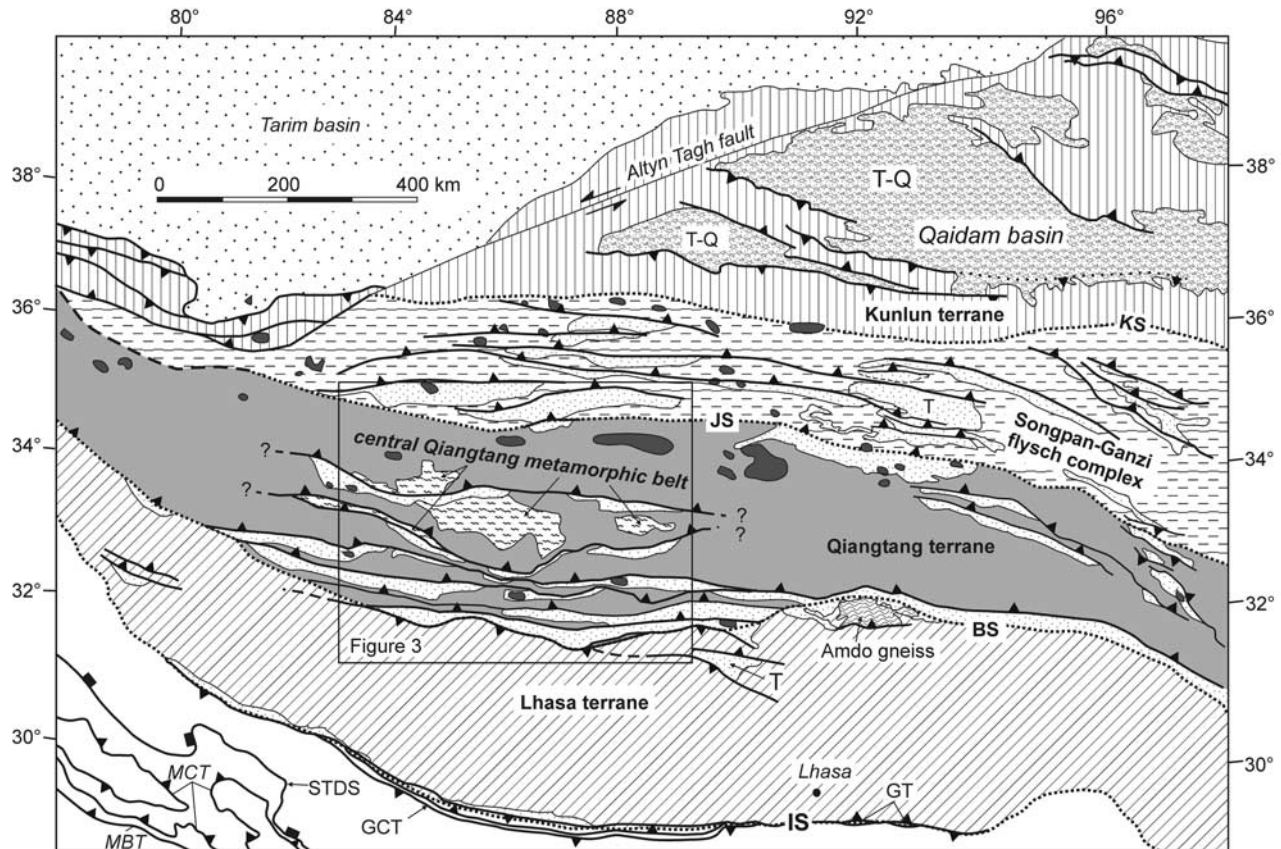


Figure 1. Tectonic map of Tibet showing locations of terranes, suture zones, major Tertiary faults and associated basinal strata; based on our mapping and interpretation of the 1:1,500,000 scale geologic map of Liu [1988]. From north to south, the sutures are: KS, Kunlun; JS, Jinsha; BS, Bangong; and IS, Indus. Abbreviations are: GCT, Great Counter thrust system; GT, Gangdese thrust system; STDS, Southern Tibetan Detachment system; MCT, Main Central Thrust; MBT, Main Boundary Thrust; T, Tertiary nonmarine strata; T-Q, Tertiary-Quaternary nonmarine strata. Late Cenozoic volcanic rocks in north central Tibet are shown in dark gray.

conformably overlain by Devonian and younger strata [Cheng and Xu, 1986]. Hsü *et al.* [1995] proposed that the CQMB is an accretionary complex that formed beneath an early Paleozoic arc in the Kunlun terrane, and which was rifted away in the Late Paleozoic. However, the CQMB must be younger than early Paleozoic because it includes metasedimentary strata that exhibit Carboniferous to Late Triassic fossils [Li and Zheng, 1993; Li *et al.*, 1995; Deng *et al.*, 1996a]. Consistent with these timing constraints and the presence of blueschists are two competing models for the tectonic significance of the CQMB (Figure 2).

[4] It has been reported that the CQMB separates upper Paleozoic strata that exhibit only warm-water faunas in the north (Cathaysian affinity; similar to the South China block) from those that include cold-water deposits and faunas in the south (Gondwanan affinity) [Wang and Mu, 1983; Fan, 1985; Li, 1987; Fan, 1988; Li and Zheng, 1993; Chen and Xie, 1994]. These reports have led numerous workers to speculate that the CQMB may represent a significant Paleotethyan suture in Tibet, and that the Qiangtang terrane may

consist of two distinct crustal fragments (Figure 2a) [Li, 1987; Kidd *et al.*, 1988; Metcalfe, 1996; Sengör *et al.*, 1988; Li *et al.*, 1995; Zhong, 1998; Zhang, 2001].

[5] An alternative hypothesis was raised based on recent studies which suggest that the CQMB consists of early Mesozoic melange and occurs in the footwall of Late Triassic–Early Jurassic domal low-angle normal (detachment) faults, structurally beneath upper Paleozoic and Triassic continental margin strata [Kapp *et al.*, 2000]. This structural setting requires the melange to have underthrust continental margin assemblages by minimum distances equal to the width of the mapped domal melange exposures (~20 km) prior to normal faulting. As melange formation and exhumation were coeval with early Mesozoic subduction along the Jinsha suture to the north, it was suggested that Qiangtang melange consists of Songpan-Ganzi flysch and underlying strata that were thrust ~200 km southward from the Jinsha suture beneath a single Qiangtang terrane of Gondwanan affinity (Figure 2b) [Kapp *et al.*, 2000; Kapp, 2001]. This model has been challenged recently by

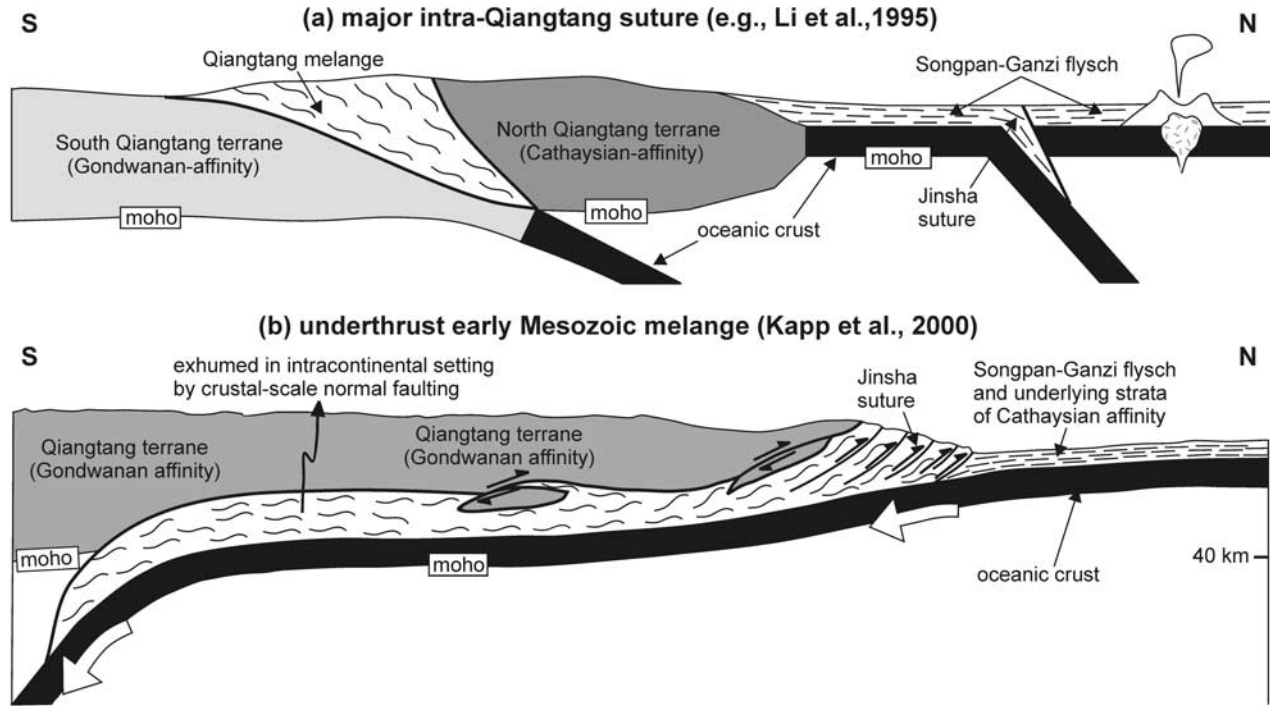


Figure 2. Competing hypotheses for the tectonic significance of the central Qiangtang metamorphic belt during early Mesozoic time.

statements that the CQMB (1) is not comprised of melange, (2) was metamorphosed 50 to 100 Myr prior to Late Triassic–Early Jurassic exhumation, and (3) did not equilibrate at the high pressures predicted by the underthrusting model [Deng *et al.*, 2001; Xia *et al.*, 2001; Zhang, 2001].

[6] Distinguishing between the in situ suture zone and melange underthrusting models is fundamental for constraining the first-order crustal structure and accretionary history of the central Tibetan plateau. Every established pre-Cenozoic suture zone in Tibet has been modified by localized Tertiary deformation and is suggested to have accommodated continental subduction or underthrusting during the Cenozoic Indo-Asian collision [Deng, 1991; Arnaud *et al.*, 1992; Matte *et al.*, 1996; Meyer *et al.*, 1998; Yin and Harrison, 2000; Tapponnier *et al.*, 2001]. Therefore if the CQMB represents a major in situ Paleotethyan suture zone, then this area should become a major target for future studies that aim to understand how India's northward penetration into Asia has been accommodated. Alternatively, if Qiangtang melange was underthrust from the Jinsha suture, ~200 km to the north, then large volumes of early Mesozoic melange may comprise the present-day deeper crust of central Tibet [Kapp *et al.*, 2000].

[7] This paper summarizes our studies on the composition, structural setting, metamorphism, and exhumation history of the CQMB. The results place constraints on the Paleozoic–Cenozoic tectonic evolution and present-day lithospheric structure of central Tibet. In addition, they provide evidence for large-scale translation of voluminous high-pressure melange beneath a continental margin during

low-angle oceanic subduction, a process which we suggest may play a more significant role in the evolution of accretionary orogens and lower continental crust than previously thought.

2. Geologic Setting

[8] From north to south, central Tibet consists of the Songpan-Ganzi flysch complex, Qiangtang, and Lhasa terranes, which are separated by the Jinsha and Bangong suture zones, respectively (Figure 1). The Songpan-Ganzi flysch complex comprises the largest volume of Triassic sedimentary rocks on Earth ($2.2 \times 10^6 \text{ km}^3$) [Nie *et al.*, 1994]. These strata are dominantly Late Triassic in age and reach 10 to 15 km in thickness [Rao *et al.*, 1987; Hou *et al.*, 1991; Nie *et al.*, 1994]. They were deposited in multiple basins [Yin and Harrison, 2000] that formed on continental margins of the North China [Zhou and Graham, 1996] and South China [Burchfiel *et al.*, 1995] blocks as well as Paleotethys oceanic lithosphere [Sengör and Okuroğullari, 1991]. However, it is generally accepted that the majority of Songpan-Ganzi flysch was derived from the Qinling-Dabie orogen [Nie *et al.*, 1994; Yin and Nie, 1996; Zhou and Graham, 1996; Bruguier *et al.*, 1997], which exposes ultrahigh pressure rocks and experienced rapid denudation during Late Triassic collision between the North and South China blocks [e.g., Hacker *et al.*, 2000b].

[9] The Lhasa and Qiangtang (at least the southern portion) terranes were likely contiguous along the margin of Gondwana during late Paleozoic time. Both terranes expose Cambrian gneiss [Xu *et al.*, 1985; Kapp *et al.*,

2000] and upper Paleozoic strata that exhibit cold-water biota and glaciomarine deposits [Yin *et al.*, 1988; Li and Zheng, 1993]. Between the Lhasa-Qiangtang terranes to the south and Eurasia to the north was the Paleo-Tethys Ocean. This ocean was consumed by northward subduction beneath the Kunlun terrane during Permo-Triassic time and southward subduction beneath the Qiangtang terrane during Late Triassic–Early Jurassic time [Dewey *et al.*, 1988; Pearce and Mei, 1988; Sengör *et al.*, 1988; Nie *et al.*, 1994; Yin and Nie, 1996]. Remnants of these northern and southern paleosubduction zones are preserved as scattered ophiolitic fragments and melanges of the Kunlun and Jinsha sutures, respectively (Figure 1) [Dewey *et al.*, 1988; Burchfiel *et al.*, 1989; Yin and Harrison, 2000].

[10] Rifting of the Qiangtang terrane from the Lhasa terrane and opening of the intervening Bangong Ocean occurred during Permo-Triassic [Sengör *et al.*, 1988] or Early Jurassic time [Yin *et al.*, 1988], contemporaneous with closure of the Paleo-Tethys Ocean to the north. The change from marine to nonmarine sedimentation within the Songpan-Ganzi basin during the earliest Jurassic is taken to record the final accretion of the Qiangtang terrane to the Eurasian margin [e.g., Dewey *et al.*, 1988]. The Bangong Ocean closed by northward subduction beneath the Qiangtang terrane and perhaps one or more oceanic island arc terranes during Middle Jurassic–Early Cretaceous time [Girardeau *et al.*, 1984; Tang and Wang, 1984; Pearce and Deng, 1988], resulting in reamalgamation of the Lhasa and Qiangtang terranes.

[11] The Qiangtang terrane was mapped at a scale of 1:1,000,000 by the Tibetan Bureau of Geology and Mineral Resources during the 1970's and early 1980's, with emphasis on stratigraphic studies [Cheng and Xu, 1986, 1987]. The regional map pattern between 80°E and 92°E is explained by the ~600-km-long and up to 270 km-wide east plunging Qiangtang anticlinorium (Figure 3) [Yin and Harrison, 2000]. It is characterized by upper Paleozoic shallow marine strata and metamorphic rocks in its core and Triassic-Jurassic shallow to nonmarine strata and volcanic rocks along its limbs. Qiangtang metamorphic rocks include mafic and metasedimentary schists and gneisses, marble, quartzite, slate, and chert [Cheng and Xu, 1986; Li and Zheng, 1993]. Blueschists were first collected from the CQMB near the Guogangjainian Shan (Figure 3) during an expedition led by Sven Hedin during 1906–1907 [Hedin, 1966] and later identified by Hennig [1915]. Subsequently, several additional blueschist localities have been documented [Cheng and Xu, 1986; Li *et al.*, 1995; Kapp *et al.*, 2000].

3. Structural Geology

[12] We conducted structural mapping (using 1:100,000 scale topographic maps) at three areas within the CQMB: near Shuang Hu (33°N, 89°E; Foldout 1), Rongma (33°N, 87°E; Foldout 2), and in the Gangma Co-Lugu area (33°N–34°N, 84°15'E; Foldout 3) (Figure 3).

3.1. Shuang Hu Area

[13] Metamorphic rocks in the Shuang Hu area were mapped as two units (Figure 4a). One unit consists of

interlayered metagraywacke, pelitic to mafic schists, quartzo-feldspathic gneiss, and marble (hereinafter referred to as the “sch” unit). It is mylonitized in most places and intruded by weakly deformed to undeformed granites and granodiorites (hereinafter referred to as “gr1”). The second unit consists of weakly foliated to unfoliated metabasites (hereinafter referred to as the “mf” unit) that include gabbros and pillow basalts, which occur as 10-m- to km-scale tectonic blocks within the sch unit.

[14] Stratigraphic successions surrounding the metamorphic rocks were divided into four units (Figure 4a). The stratigraphically lowest unit is a dolostone that includes Late Triassic fossils (hereinafter referred to as “Tra”) [Cheng and Xu, 1986]. Conformably overlying Tra is a volcanic-bearing unit (hereinafter referred to as “Trb”), which is in turn capped by a limestone-bearing unit (“Trc”). Units Trb-Trc are assigned a Late Triassic age, following Cheng and Xu [1986]. A limestone-clast conglomerate marks an unconformity between Trc and an overlying >3 km-thick succession of fluvial deposits (Trd1–Trd4). Although originally assigned a Tertiary age [Cheng and Xu, 1986], our mapping and timing constraints on the Falong detachment, described below, suggest a Late Triassic–earliest Jurassic age for the Trd unit.

[15] Metamorphic rocks occur in the footwall of a domal low-angle normal fault, the Falong detachment, which juxtaposes them against Triassic strata and granitoids in the hanging wall (Foldout 1) [Kapp *et al.*, 2000]. Triassic strata are repeated by the Qiage La thrust system, which is interpreted to be cut by the Falong detachment. Both the Falong detachment and the Qiage La thrust system are cut by late Cenozoic high-angle normal faults [Yin *et al.*, 1999]. These fault systems and associated structures and fabrics are described from oldest to youngest.

3.1.1. Qiage La Thrust System

[16] The Qiage La thrust system consists of three, ~NE striking thrust faults (Foldout 1). The two westernmost thrusts place dolostone (Tra) in the hanging wall over the Trb unit in the footwall. Strata in the footwall of the thrust fault southwest of Qiage La (La is Tibetan for pass) are metamorphosed to greenschist facies and exhibit a foliation and NW to SW plunging stretching lineations that become progressively stronger toward the fault. The dolostone directly above the fault exhibits asymmetric boudinage that indicates top-to-the-southwest sense-of-shear. The easternmost thrust fault places the Tra and Trb units over red beds (Trd4) in the footwall that are internally deformed by north striking thrusts and gently north plunging folds. Minimum slip on the individual thrust faults is between 1.5 and 4.5 km, based on the amount of stratigraphic throw across them. We could not trace the Qiage La thrust system into the sch unit, and therefore interpret it to be cut by the Falong detachment [Kapp *et al.*, 2000].

3.1.2. Falong Detachment

[17] The Falong detachment is well exposed at several localities. At locality 97-6-17-3 (Foldout 1), hanging wall dolostone is deformed by ~S70°E-vergent asymmetric folds and east dipping normal faults (Figure 5a) [Kapp *et al.*, 2000]. Directly beneath the detachment is a 10- to

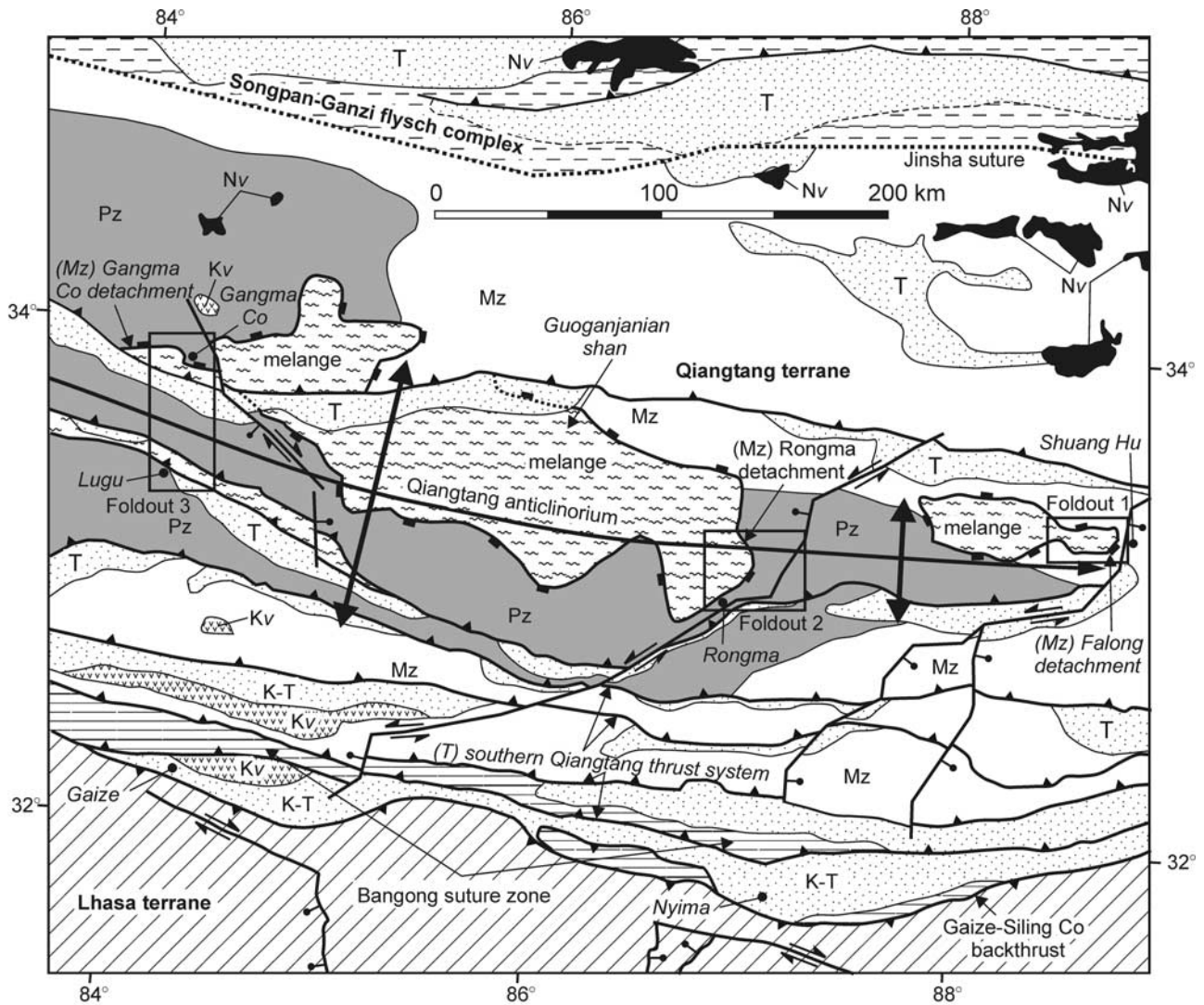


Figure 3. Tectonic map of the Qiangtang terrane based on our mapping and interpretations of the 1:1,000,000 geologic map of the Gaize region [Cheng and Xu, 1986]. Abbreviations are: Pz, upper Paleozoic shallow marine strata; Mz, Mesozoic strata; Kv, Cretaceous volcanic rocks; K-T, Cretaceous-Tertiary (undivided) nonmarine strata; T, Tertiary nonmarine strata. The Bangong suture zone (horizontal rule) is comprised of Jurassic flysch, melange (some containing mafic gabbro and ultramafic fragments), and volcanic rocks.

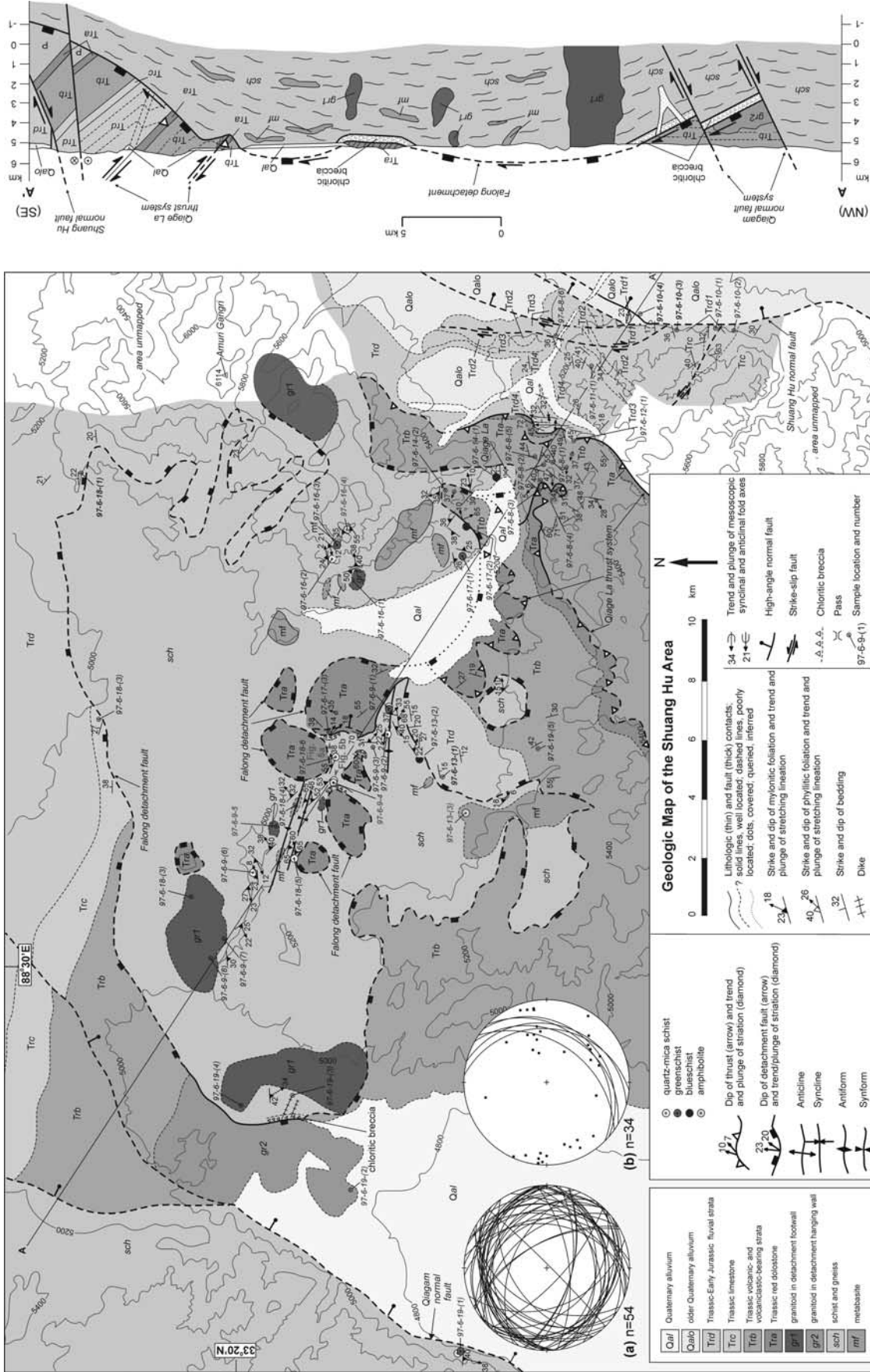
20-m-thick ledge of chloritic breccia that grades structurally downward into mylonitic schists and gneisses (Figures 5a–5c). To the west near locality 97-6-19-3, the Falong detachment cuts an unfoliated ~220 Ma granitoid in its hanging wall [Kapp et al., 2000]. Just northwest of Qiage La, at locality 97-6-17-2, the Falong detachment exhibits east plunging striations and juxtaposes mafic schists in the footwall against the Trb unit in its hanging wall.

[18] Footwall foliations dip gently to moderately and in variable directions (Foldout 1a). In general, stretching lineations plunge gently both to the east and west (Foldout 1b). They are subparallel to striations measured on the detachment fault surface and to the poles of normal faults in Triassic strata directly above the detachment (Foldout 1b), suggesting that the footwall mylonitic fabric is kinematically

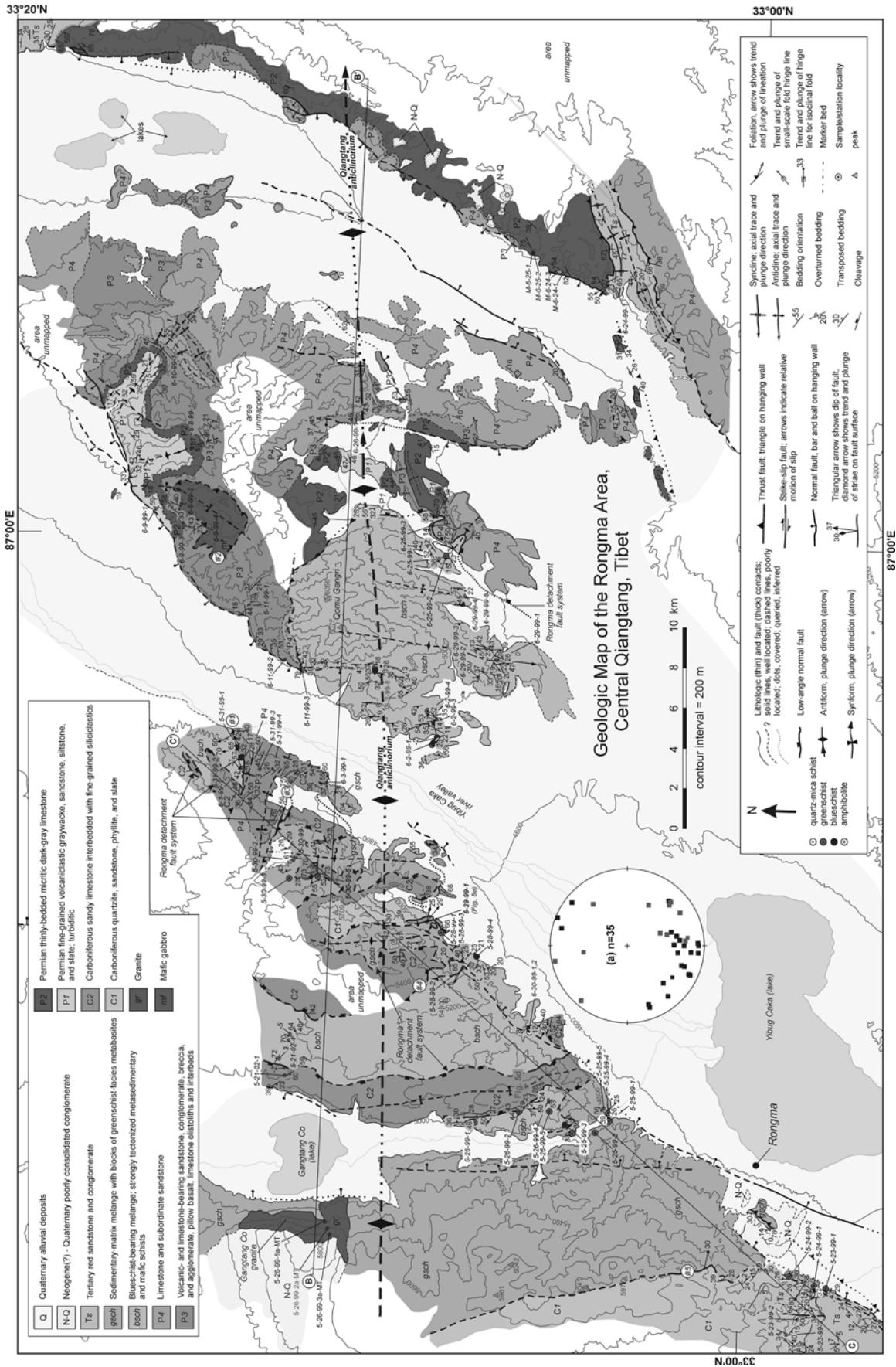
related to detachment faulting [Kapp et al., 2000]. Mesoscopic asymmetric folds, ductile normal faults, kink bands, and S-C fabrics (Figure 5c) within the footwall indicate detachment faulting with E-SE displacement of the hanging wall relative to the footwall. Orientations of footwall foliations define corrugations subparallel to the transport direction of the detachment. Minimum slip along the detachment is ~20 km, based on the width of its exposed footwall in map view (Foldout 1).

3.1.3. Shuang Hu and Qiagam Normal Faults

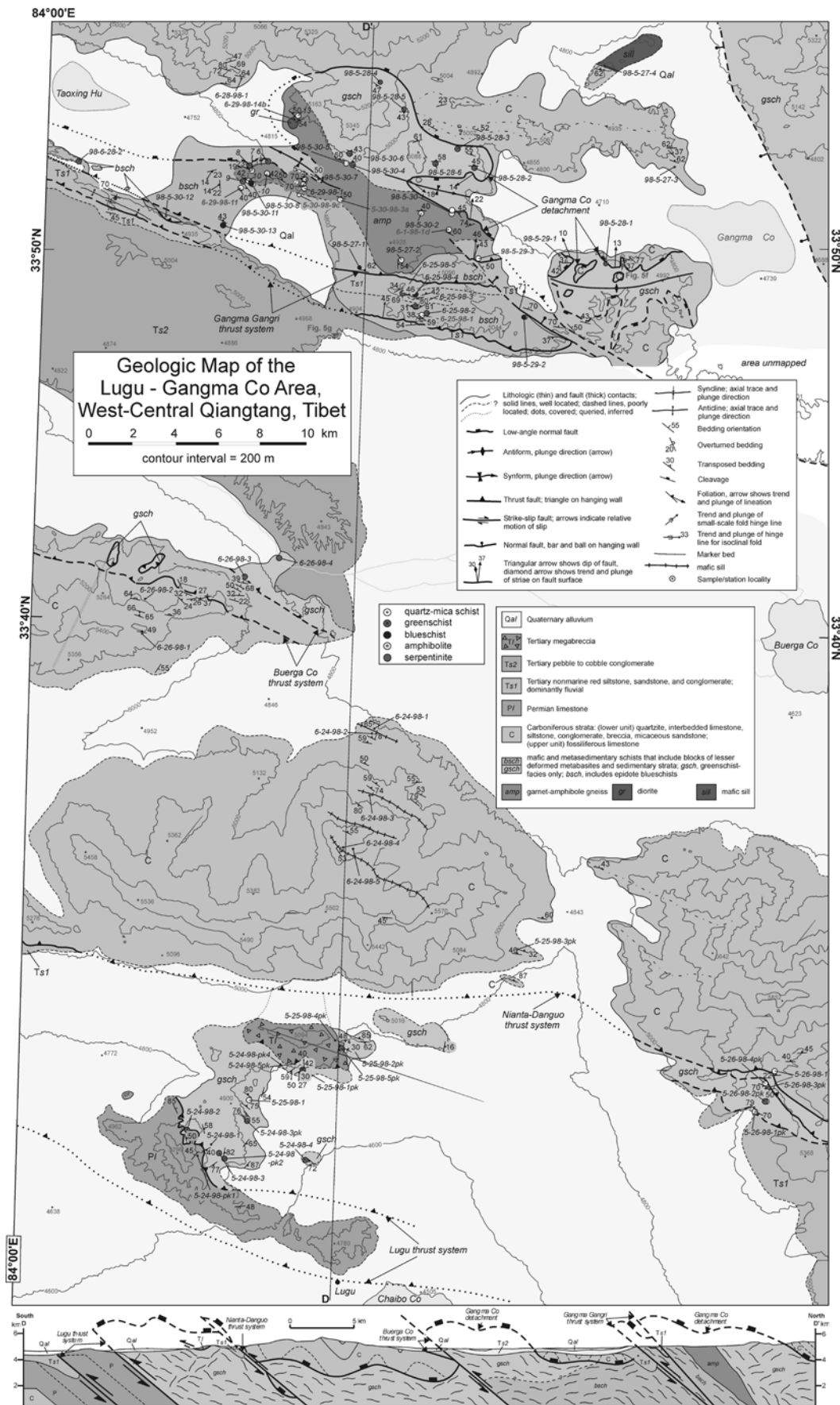
[19] Major north to NE trending topographic highs in the Shuang Hu area are bound on their southeast flanks by late Cenozoic normal fault systems (Foldout 1) [Yin et al., 1999]. To the west, the Qiagam normal fault system bounds the western margin of a Quaternary lacustrine basin. In the



Foldout 1. Geologic map and cross section of the Shuang Hu area modified from Kapp *et al.* [2000]. Red arrows show locations and directions of view for photos in Figures 5a–5c. Localities of geochronologic samples are shown in red. Pebble imbrications were measured at the localities shown in blue. Lower hemisphere, equal-area stereonet shows measured (a) planes of foliation and (b) stretching lineations in footwall schists of the Falong detachment and orientations of normal faults that cut Triassic strata directly above the Falong detachment at locality 97-6-17-3 (shown as planes). See enlarged version of this figure in the HTML.



Foldout 2. Geologic map of the Rongma area. See Figure 6 for cross sections along the lines B–B’ and C–C’. Localities of geochronologic samples are shown in red. Red arrows show locations and directions of view for the photos shown in Figures 5d–5e. Lower hemisphere, equal-area stereonet show measured (a) stretching lineations of schists within the footwall of the Rongma detachment to the west (black circles) and east (red circles) of the Yibug Caka river valley. See enlarged version of this figure in the HTML.



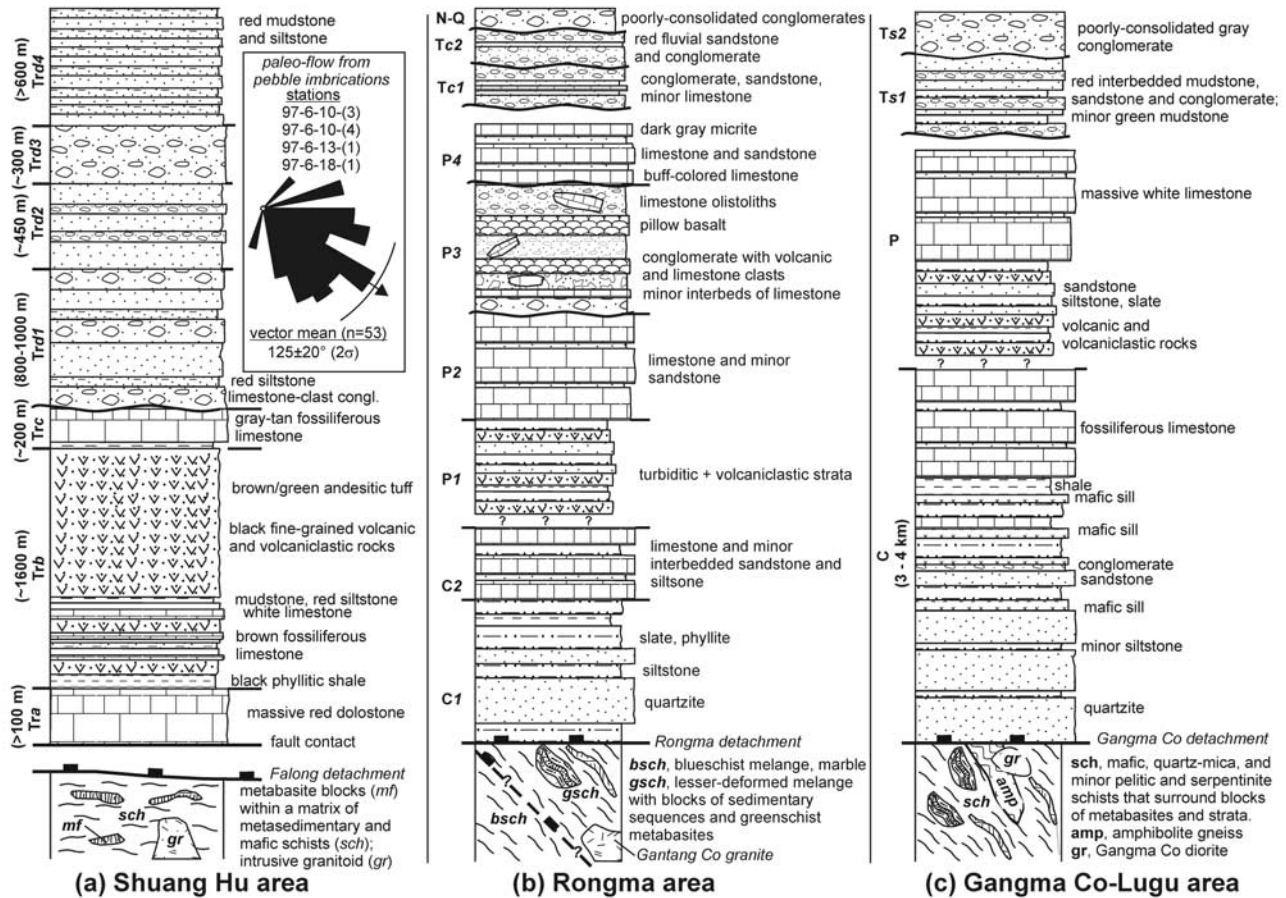


Figure 4. Structural-stratigraphic columns for the (a) Shuang Hu, (b) Rongma, and (c) Gangma Co-Lugu areas. Abbreviations are: C, Carboniferous, P, Permian; Tr, Triassic; T, Tertiary, N-Q, Neogene-Quaternary.

east, the Shuang Hu normal fault system obliquely cuts the bedding of Triassic strata, and in some places, juxtaposes them against Quaternary alluvial deposits (Qalo). The total magnitude of slip across the Shuang Hu normal fault system is ~ 7.0 km [Yin *et al.*, 1999].

3.2. Rongma Area

[20] In the Rongma area, Carboniferous-Permian shallow marine strata and metamorphic rocks are well exposed along the flanks of the active NE trending Yibug Caka (“Caka” is Tibetan for salt lake) rift system [Taylor *et al.*, 2003] (Figure 5d). Fluvial clastics (Tc) correlated with the Tertiary Kangtuo formation [Cheng and Xu, 1986] are exposed to the north and south of the metamorphic rocks (Foldout 2). Additionally, gently dipping Neogene-Quaternary poorly consolidated conglomerate (N-Q) is exposed locally on tops of the rift flanks and within the rift system.

[21] Age assignments for Paleozoic strata follow those of Li *et al.* [1995]. Carboniferous strata include a lower quartzite-bearing unit (C1) and an upper limestone-bearing unit (C2) (Figure 4b). The stratigraphically lowest Permian unit, P1, consists of turbiditic sandstone and volcanoclastic rocks. It is overlain by a limestone-bearing unit, P2, which is in turn unconformably overlain by mafic volcanic- and limestone-clast conglomerate, sandstone, breccia, and agglomerate, which are interbedded with pillow basalt and limestone (P3) (Lower Permian Rongma formation of Li and Zheng [1993]). Unconformably overlying P3 is a >400-m-thick sequence of interbedded limestone and sandstone, P4. Thinly bedded upper Paleozoic strata are cleaved and locally, tightly folded.

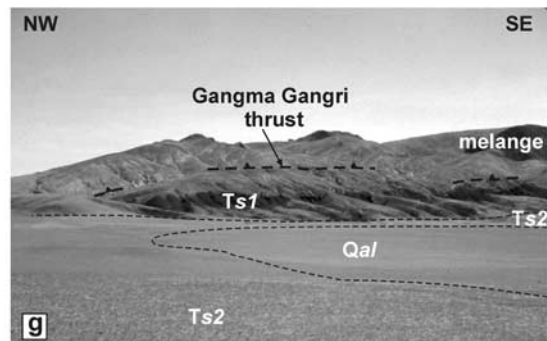
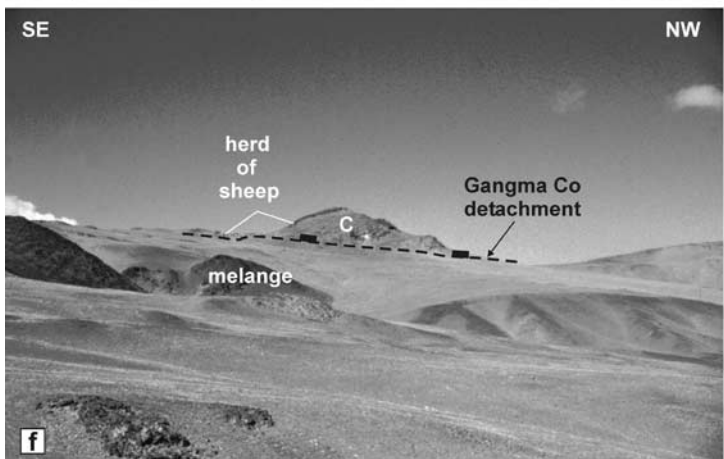
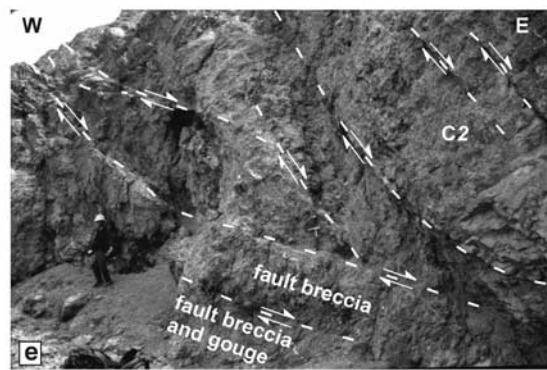
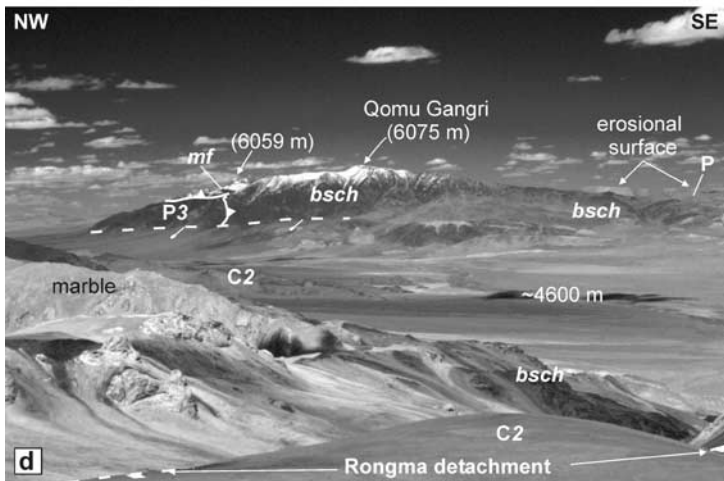
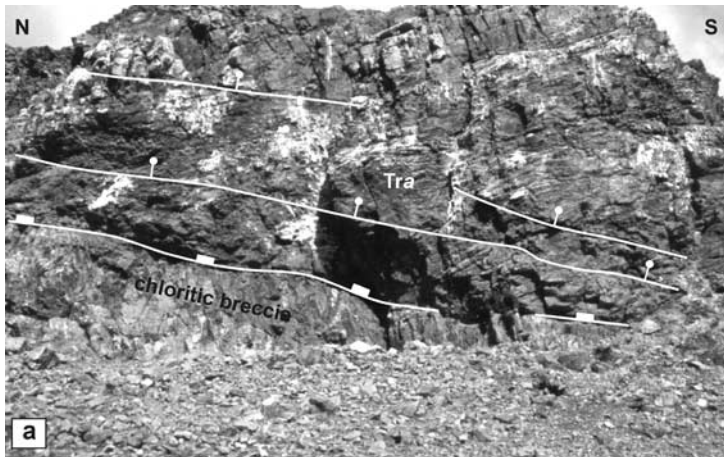
[22] The two metamorphic map units are distinguishable based on the extent of ductile deformation and the presence or absence of sodic amphibole in mafic schists. The “gsch” unit is characterized by a matrix of strongly cleaved and tightly folded, but only locally tectonized, metasedimentary

Foldout 3. (opposite) Geologic map and cross section (D–D’) of the Lugu-Gangma Co area. The map of the Gangma Co area is modified from Kapp *et al.* [2000]. Geochronologic sample localities are shown in bold red. Red arrows show locations and directions of view for photos shown in Figures 5f–5g. See enlarged version of this figure in the HTML.

and greenschist-facies metamafic rocks. Chaotically distributed within the matrix are lesser-deformed 100-m- to km-scale tectonic blocks of (1) greenschist-facies metabasites and minor ultramafic rock, (2) metabasite- and limestone-clast conglomerate and breccia, and (3) metasedimentary rocks that are similar in lithology to nearby Carboniferous-Permian stratigraphic sequences. The gsch unit is intruded

by the undeformed, two-mica-bearing Gangtang Co granite (Foldout 2).

[23] The “bsch” unit consists of a strongly tectonized metamafic to metasedimentary matrix that surrounds 10-m- to km-scale lenses of foliated marble (Figure 5d). Some metasedimentary rocks within the matrix are comprised of lithologies that are similar to those of nearby upper Paleo-



zoic strata. Mafic schists contain sodic amphibole, which together with chlorite, give a blue color to this unit. Quartz-calcite veins are ubiquitous and appear to have been injected during foliation development. An additional map unit, "mf," is an undeformed olivine-bearing gabbro.

3.2.1. Rongma Detachment

[24] The oldest structure mapped in the Rongma area is the Rongma detachment, which is characterized by a zone of fault breccia and gouge that separates footwall metamorphic rocks from hanging wall Paleozoic strata (Foldout 2). At locality 6-25-99-3, the fault breccia is >20-m thick and is composed mostly of footwall schists. Permian conglomerates (P3) directly above the detachment are deformed by numerous meter-scale NW and SE dipping normal faults. At localities 5-29-99-1 and 5-30-99-5, a 1- to 2-m-thick zone of fault breccia and gouge separates hanging wall Carboniferous limestones (C2) from footwall metabasites of the gsch unit. Directly above the detachment, limestones are cut by SE dipping listric normal faults that root into the low-angle fault zone (Figure 5e). Orientations of striae and roll-over anticlines associated with the normal faults suggest nearly pure dip-slip displacement. Shear fabrics within the fault breccia are indicative of transport of the hanging wall to the southeast relative to the footwall. In the eastern part of the map area, Permian strata comprise a >30-km-long and >4-km-wide, steeply NW dipping tilt block (Foldout 2). Tertiary red beds that lie unconformably above or structurally below these Permian strata are not tilted westward. Thus, the tilt block could not have formed during late Cenozoic extension. We attribute westward tilting to hanging wall rotation along an east dipping normal fault which roots structurally downward into the Rongma detachment, but is now buried beneath Quaternary alluvium (Figure 6a). A minimum slip of ~40 km for the Rongma detachment is suggested from the map-view width of footwall metamorphic exposures in the direction of transport (Foldout 2).

[25] The Rongma detachment and its footwall are warped into antiforms and synforms with hinge lines that plunge variably to the north and south, and with a wavelength of 2 to 4 km (Foldout 2). As there is no evidence for regional E-W shortening, we suggest that these warps are related to

detachment faulting. While the mechanism of their formation is unclear, small-wavelength extension-perpendicular warps have been documented within North American metamorphic core complexes [e.g., *Yin and Dunn, 1992*].

[26] It is uncertain whether fabrics in the detachment footwall are related to normal faulting or older deformation. On average, foliations strike, and lineations trend, roughly N-S. Lineations exhibit a slight change in trend across the Yibug Caka river valley (Foldout 2, stereonet "a"). To the west, half of the measured lineations trend SE or NW, subparallel to the transport direction of the Rongma detachment. In contrast, the bsch unit exposed on Qomu Gangri (Gangri is Tibetan for snow mountain) exhibits stretching lineations that trend more NE-SW. Fabrics in footwall schists are heterogeneous; they include L-tectonites, symmetric boudinage, and composite shear fabrics that indicate variable sense-of-shear directions.

3.2.2. Postdetachment Structures

[27] The Rongma detachment is cut by numerous faults (labeled "1" in the north to "5" in the south; Foldout 2) that predate late Cenozoic rifting and place metamorphic rocks in their hanging wall against upper Paleozoic strata in their footwall. The timing and kinematics of these faults are poorly constrained. However, a NE-SW cross section suggests that they accommodated minimal shortening (~6 km across the 39-km-long cross section) and exhumation of the metamorphic rocks (Figure 6b).

[28] The axial trace of the Qiangtang anticlinorium trends E-W across the middle of the map area (Foldout 2). The anticlinorium deforms the Rongma detachment and hanging wall Permian strata. Tertiary red beds that lie unconformably on the northern margin of the west dipping tilt block of Permian strata are north to NE dipping, whereas the unconformity below Tertiary red beds west of Rongma is gently south dipping. These observations indicate growth of the anticlinorium during the Tertiary. In the southeastern part of the map area, Tertiary strata occur in the footwalls of a NW dipping thrust to the north and a SE dipping thrust fault to the south. These conjugate thrust faults may have formed as a consequence of a buckling instability during anticlinorium development.

Figure 5. (opposite) (a) View to east at Falong detachment near locality 97-6-13-3 (Foldout 1). Hanging wall normal faults dip into the plane of the photo. (b) View to west at 10–20-m-thick zone of chloritic breccia directly beneath Falong detachment near locality 97-6-9-4 (Foldout 1). It grades structurally below into light-colored mylonitic schists and gneisses. (c) View to north at mylonitic S-C fabrics in the footwall of the Falong detachment which indicate top-to-the-ESE sense-of-shear. (d) View to northeast across Yibug Caka river valley at Qomu Gangri peak in the Rongma area (Foldout 2). In the foreground, the Rongma detachment juxtaposes hanging wall Carboniferous limestone, C2, against footwall blueschist-bearing melange, bsch, with blocks of marble. Abbreviations: P, Permian strata, undivided; P3, Permian mafic volcanic rocks and conglomerates; mf, mafic gabbro. The prominent river valley and elevated erosional surface in background are related to the late Cenozoic Yibug Caka rift system [*Taylor et al., 2003*]. (e) View to north at locality 5-29-99-1 in the Rongma area (Foldout 2). Several listric normal faults within Carboniferous limestone, C2, root into a low-angle zone of fault breccia and gouge, which characterizes the Rongma detachment. Structurally below is metabasite-bearing melange. (f) View to southwest near locality 98-5-28-1 at the Gangma Co detachment (Foldout 3). Here, it is defined by a low-angle zone of dark fault breccia directly beneath tilted Carboniferous limestone, C, in the hanging wall. Footwall lithologies include mafic schist and weakly foliated metabasites. (g) View to northeast at the southernmost thrust of the Gangma Gangri thrust system (Foldout 3). Here, it places variably deformed metabasites (in black) that occur as tectonic blocks within a matrix of light-colored quartz-mica schist on top of Tertiary red beds. Some metabasites in this photo exhibit epidote-blueschist facies mineral assemblages. See color version of this figure at back of this issue.

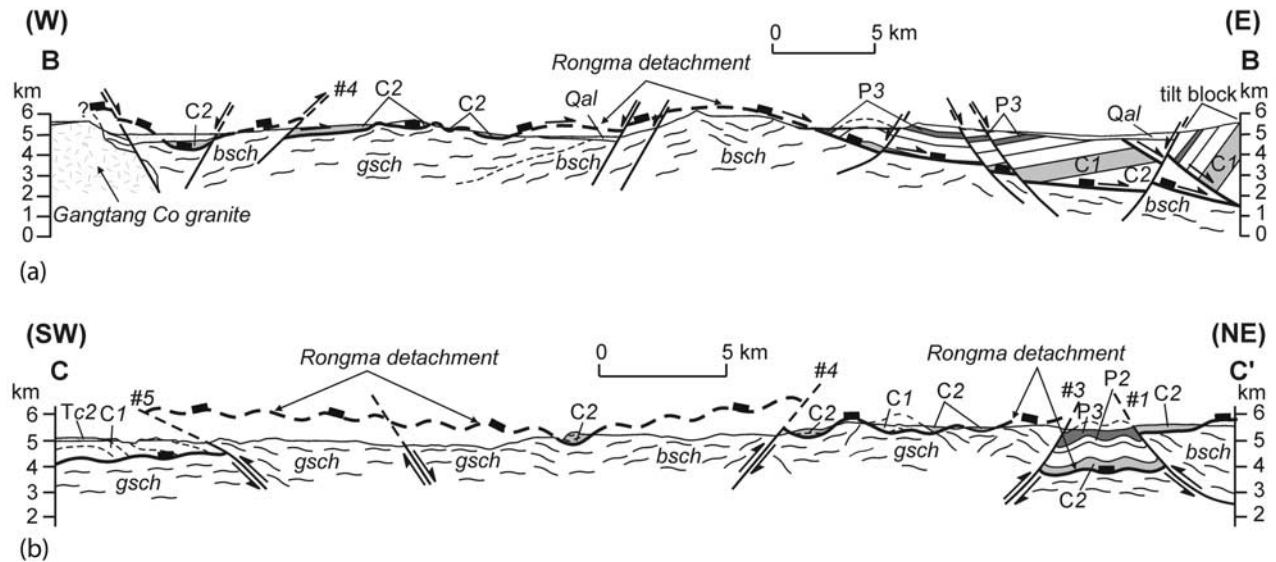


Figure 6. (a) East-west, B–B'; Early Mesozoic normal faults are bolder than younger faults and (b) northeast-southwest, C to C' cross sections of the Rongma area. See Foldout 2 for lines of section and unit abbreviations. Abbreviations are: gsch, greenschist-facies melange; bsch, blueschist-facies melange; C1, Carboniferous quartzite-bearing siliciclastic rocks; C2, Carboniferous limestone-bearing strata; P1, Permian turbiditic sandstone; P2, Permian limestone; P3, Permian mafic volcanic rocks and conglomerates; P4, Permian limestone and sandstone; Ts2, Tertiary nonmarine strata; N-Q, Neogene-Quaternary conglomerate; Qal, Quaternary alluvium.

[29] North to NE striking range-bounding normal faults of the late Cenozoic Yibug Caka rift system cut Quaternary alluvium, are associated with prominent fault scarps, and accommodated ~NW-SE extension [Taylor *et al.*, 2003]. It is difficult to precisely constrain the magnitude of slip across several of the major range-bounding normal faults due to the lack of preserved cutoffs. However, a W-E cross section across the ~50-km-wide Yibug Caka rift system suggests that a minimum of ~2 km of E-W extension is required to produce the observed map relationships (Figure 6a). To both the southwest and northeast beyond the map area, the rift system is kinematically linked with active N70°E striking left-lateral strike-slip faults [Taylor *et al.*, 2003] (Figure 3).

3.3. Lugu-Gangma Co Area

[30] Metamorphic rocks in the Lugu-Gangma Co area were mapped as three units (Figure 4c). The bsch and gsch units consist of a matrix of metagraywacke and mafic, quartz-mica, and minor serpentinite schists that surround lesser-deformed blocks of metabasites and metasedimentary rocks. Matrix mafic schists and metabasite blocks of the bsch unit exhibit greenschist and epidote-blueschists facies mineral assemblages, whereas those of the gsch unit exhibit only greenschist facies mineral assemblages. In both units, the mafic schists are foliated, but stretching lineations are either weak or absent. Locally, quartz-mica schists exhibit a weak stretching lineation. The “amp” unit is a ~10-km-long and ~2-km-wide, semi-coherent block of well-banded

mafic gneiss. The gneiss becomes finer-grained and more deformed toward its contacts with the sch unit, suggesting that the latter are tectonic. The gneiss is intruded by a diorite (gr) that is <1 km in diameter.

[31] Upper Carboniferous strata of the Zhanjin formation are widely exposed in the Gangma Co-Lugu area [Cheng and Xu, 1986; Li and Zheng, 1993]. Based on our mapping, these strata (C) are 3- to 4-km-thick and consist of a lower part of quartzite, a middle part of interbedded limestone and fine-grained clastics that is intruded by mafic sills, and an upper part of fossiliferous limestone (Figure 4c). Permian strata (P1) (Lugu formation) [Cheng and Xu, 1986; Li and Zheng, 1993] consist of interbedded siliciclastic, volcanic, and volcaniclastic rocks that are overlain by limestone. Thinly bedded upper Paleozoic strata are deformed by mesoscopic tight and isoclinal folds and bedding-parallel cleavage. Quartzites are weakly foliated in places, whereas the massive limestones are broadly folded and exhibit spaced cleavage. Tertiary strata of the Kangtuo formation [Cheng and Xu, 1986] include fluvial red clastics (Ts1) and unconformably overlying, poorly consolidated conglomerates (Ts2). Near Lugu, Tertiary strata include a monolithologic (quartzite) megabreccia (T1).

3.3.1. Gangma Co Detachment Fault

[32] The Gangma Co detachment [Kapp *et al.*, 2000] is characterized by a subhorizontal zone of dark fault breccia and gouge that exceeds 10 m in thickness. Just west of Gangma Co, it places Carboniferous limestone in the hanging wall against the gsch unit in the footwall (Figure 5f). Footwall foliation strikes E-W and in the

few places where stretching lineations are present, they plunge to the SW. At locality 5-28-98-1, Carboniferous limestone directly above the detachment is cut by north dipping brittle normal faults that exhibit striae trending N40°E to N48°E. Additional structural data are necessary to better constrain the kinematics of the detachment fault.

3.3.2. Tertiary Faults

[33] Four north dipping thrust systems, spaced ~10–14 km apart, were mapped in the Lugu-Gangma Co area (Foldout 3). From north to south, they are the Gangma Gangri, Buerga Co, Nianta-Danguo, and Lugu thrust systems. The Gangma Gangri thrust system (Figure 5g) cuts the Gangma Co detachment fault and includes Tertiary red beds in its footwall. The thrust faults exhibit north trending striae and hanging wall strata are deformed by mesoscopic south vergent folds. The northern thrust of the Buerga Co thrust system places the gsch unit on top of Carboniferous strata in its footwall, whereas the southern thrust fault repeats Carboniferous strata. Slip along the Buerga Co thrust system occurred prior to deposition of the T_s2 unit, which is nearly flat-lying less than 2 km north of the thrust system. Tertiary red beds and a megabreccia unit (TI), interpreted to be a landslide deposit, occur in the footwall of the Nianta-Danguo thrust system, with Carboniferous strata and the gsch unit in the hanging wall. The northern thrust of the Lugu thrust system places the gsch unit on top of Permian strata. A series of en echelon quartz veins directly above the fault are compatible with south directed thrusting. To the south, a north dipping thrust fault is mapped as buried, having been projected from beyond the map area to the west where it repeats a section of Permian limestone and unconformably overlying Tertiary red beds.

[34] The Gangma Co detachment occurs in the footwall of the Gangma Gangri thrust system beyond the map area to the east. We infer that metamorphic rocks to the south also occur in the footwall of a detachment fault which is either tectonically buried in the footwall of the thrust systems or has been denuded. The repetition of upper Paleozoic strata and metamorphic rocks indicates relatively small magnitudes of throw across the thrust systems. A tentative 99 km-long N-S cross section suggests that the thrust systems accommodated a ~28 km (~22%) shortening (Foldout 3).

[35] The Gangma Co detachment and Gangma Gangri thrust system are cut by two NW striking high-angle normal faults. The western fault is NE dipping and down-drops Tertiary red beds against the sch unit (Foldout 3). To the east of Gangma Co, a W-SW dipping normal fault juxtaposes the sch unit in its footwall against Quaternary alluvium and Carboniferous strata in its hanging wall. These normal faults are strands of the late Cenozoic Chagd normal fault system [Yin *et al.*, 1999].

4. Metamorphism

[36] Compositions of amphibole in CQMB blueschist indicate relatively high-P/low-T conditions characteristic of subduction zone settings [Li *et al.*, 1995; Bao *et al.*, 1999; Kapp *et al.*, 2000]. However, quantitative P-T estimates are lacking. In this section, we summarize mineral

assemblages and present the first thermobarometric results for the CQMB.

4.1. Petrography

[37] Mineral assemblages in 165 samples from the CQMB are listed in Table A1 (available as auxiliary material)¹ and represented on Foldouts 1, 2, and 3 by colored circles. Mineral abbreviations are from Kretz [1983], except for amphibole (Amp) and phengite (Phe). Metasedimentary rocks exhibit similar mineral assemblages throughout the CQMB: Qtz + Ms-Phe(?) ± Pl ± Ep ± Chl ± Bt ± Cal ± Grt ± Ap ± Sph ± Rt. In contrast, mineral assemblages exhibited by matrix mafic schists and metabasite blocks vary significantly within the CQMB and are described below.

[38] Greenschist-facies mafic schists and weakly foliated metabasite blocks are ubiquitous in the CQMB. The metabasite blocks may preserve primary igneous textures, and contain the assemblage: Chl + Sph + Pl + Qtz + Ep ± calcic Amp ± Rt ± Stp ± Bt ± Ms ± Cal ± relict igneous Cpx ± Hbl ± Ol (replaced by Tlc + Atg) ± Ap. The mafic schists exhibit the same mineral assemblage as the greenschist-facies metabasite blocks, except that hornblende is absent and garnet may be present.

[39] Epidote-blueschist facies mafic schists and metabasite blocks were identified in all areas, except near Lugu. Those near Shuang Hu are nearly completely retrograded by greenschist-facies mineral assemblages. Qiangtang epidote blueschists are distinguished from mafic greenschists by the presence of sodic amphibole: Chl + Sph + Pl + Qtz + Ep + sodic Amp ± calcic Amp ± Stp ± Bt ± Phe ± Cal ± relict igneous Cpx ± sodic Cpx (Gangma Co area only) ± Grt (Rongma area only) ± Rt ± Ap. Actinolite occurs as rims or overgrowths on sodic amphibole, in samples where both amphiboles are present.

[40] Epidote-amphibolite facies metabasite blocks (calcic Amp + Qtz + Pl + Ep + Sph ± igneous Cpx ± Bt ± Chl ± Rt ± Ap) and mafic schists (calcic Amp + Qtz + Pl + Chl + Ep + Sph + Rt ± Grt ± Bt) are common in the Shuang Hu area. Near Gangma Co, the *amp* unit contains the assemblage: calcic Amp + Pl + Qtz + Sph ± Ep ± Grt ± Rt. The abundances of amphibole and epidote increase, at the expense of garnet, toward the more schistose portions of the gneiss. As concluded below, the metamorphism of the *amp* unit significantly predates and is unrelated to that of the remainder of the CQMB.

4.2. Thermobarometry

[41] Mineral compositions were obtained using a Cameca Camebax electron microprobe with four wavelength-dispersive spectrometers at the University of California, Los Angeles. A beam diameter of 1 to 3 μm was used for all minerals except for plagioclase, mica, and chlorite, for which a slightly defocused beam with a diameter of 5 to 6 μm was used. An accelerating voltage of 15 kV and a sample current of ~10 nA were used. Counting times for all

¹ Supporting Tables A1–A5 are available at <http://agu.org/apend/tc/2002TC001383>. Information on searching and submitting auxiliary material is found at http://www.agu.org/pubs/esupp_about.html.

elements were 20 s. Compositional data were normalized and phase activities were calculated using the schemes listed in Table A2 and representative or mean mineral compositions are listed in Table A3 (see auxiliary material). All phase equilibria calculations were performed using the TWEEQU program of *Berman* [1991], and an updated thermodynamic data set (JUN92.GSC) of *Berman* [1988].

4.2.1. Epidote Blueschist

[42] Three samples of Gangma Co blueschist include the assemblage: Pl + Ph + Chl + Qtz + Ep + Ttn + Rt + omphacitic Cpx. A minimum P of ~10 kbar at ~350°C and ~11.5 kbar at ~450°C is provided by the equilibrium $Ab = Jd + Qtz$, calculated using the composition of omphacitic clinopyroxene in sample 5-30-98-11f and assuming that plagioclase is pure albite (Figure 7). Slightly higher (1 to 2 kbar) minimum P estimates are obtained from the phengite barometer of *Massonne and Schreyer* [1987], using homogeneous phengite compositions in samples 5-30-98-11e and 5-30-98-13a (3.49 Si per formula unit) and 5-30-98-11f (3.52 Si per formula unit). For these same samples, the chlorite-muscovite thermometer [*Powell and Evans*, 1983; *Bucher-Nurminen*, 1987] provides maximum T estimates of ~400°C at 10 kbar and ~450°C at 15 kbar, using mean activity values. These results, in addition to minimum T constraints provided by the absence of lawsonite [*Evans*, 1990], suggest $P > 10$ kbar at $425 \pm 50^\circ\text{C}$ (Figure 7).

[43] A sample of Rongma epidote blueschist (6-30-99-2d) contains the assemblage: Grt + Gl + Chl + Phe + Czo + Pl + Sph + Rt + Ilm + Qtz. Garnet is euhedral (~1 mm in diameter), grew subsequent to fabric development, and is commonly rimmed by chlorite and phengite. It is almandine-rich and exhibits prograde growth zoning, with the pyrope and grossular component increasing from core to rim. Phengite barometry [*Massonne and Schreyer*, 1987] provides a minimum P of 10 kbar at ~400°C and 11 kbar at ~500°C (Figure 7). Garnet-phengite thermometry [*Green and Hellman*, 1982] provides a maximum temperature boundary that lies close to the high-T boundary of the epidote-blueschist facies calculated by *Evans* [1990] for glaucophane-bearing metabasites. Two important reactions for garnet production in epidote blueschists were calculated using mean mineral compositions (Table A3): (1) $19\text{Gln} + 6\text{Czo} + 19\text{Qtz} = 38\text{Ab} + 9\text{Prp} + 6\text{Tr} + 16\text{H}_2\text{O}$, and (2) $19\text{Chl} + 38\text{Qtz} + 4\text{Czo} = 25\text{Prp} + 4\text{Tr} + 74\text{H}_2\text{O}$. Assuming a water activity of 1.0, these reactions provide intersections at 13.6 kbar, 487°C and 14.3 kbar, 520°C using garnet core and rim compositions, respectively, which lie within the acceptable P-T range constrained by calibrated thermobarometers and the pressure-limiting reaction $Ab = Jd + Qtz$ (Figure 7). The reactions are not strongly sensitive to water activity; a water activity of 0.9 yields intersections that are shifted to lower T by ~10°C and lower P by <0.3 kbar.

4.2.2. Shuang Hu Epidote Amphibolite

[44] Thermobarometric studies were conducted on a sample (6-16-97-4a) of mylonitized epidote-amphibolite facies mafic schist from the extensional shear zone in the footwall of the Falong detachment. The sample contains the assemblage: Hbl + Grt + Pl + Czo + Qtz + Rt + Sph. Garnet occurs as porphyroclasts and is commonly rimmed by rotated tails

of hornblende. Inclusion trails in plagioclase indicate recrystallization during mylonitization. Hornblende-plagioclase thermometry [*Holland and Blundy*, 1994] and garnet-hornblende-plagioclase barometry [*Kohn and Spear*, 1990] suggest equilibration at ~660°C and ~11 kbar (Figure 7).

4.2.3. Gangma Co Gneiss

[45] Two analyzed samples of the Gangma Co gneiss (amp unit) contain the mineral assemblage: Amp + Pl + Grt + Qtz + Ep + Sph. Amphibole is tschermakite and garnet is almandine rich (Table A2). P-T conditions were estimated using garnet-hornblende-plagioclase barometry [*Kohn and Spear*, 1990] and hornblende-plagioclase thermometry [*Holland and Blundy*, 1994]. Sample 5-27-98-2c yields pressures of 4 to 7 kbar at temperatures between 675 and 825°C, suggestive of upper-amphibolite facies metamorphic conditions. Sample 6-29-98-2 yields higher pressures (6 to 9 kbar) at slightly lower temperatures (650° to 775°C).

5. Geochronology

[46] Published geochronologic studies suggest that Qiangtang detachment faulting occurred during Late Triassic–Early Jurassic time and that the Gangma Co gneiss crystallized during Early Cambrian time [*Kapp et al.*, 2000]. Here, we present U-Pb and $^{40}\text{Ar}/^{39}\text{Ar}$ results that, in conjunction with thermobarometric studies, provide additional constraints on the metamorphic and cooling histories of the CQMB. In addition, we present a U-Pb detrital zircon provenance study of Qiangtang metasedimentary rocks.

5.1. Methods

[47] Mineral separates for $^{40}\text{Ar}/^{39}\text{Ar}$ analysis were irradiated at the Ford Reactor, University of Michigan, along with Fish Canyon sanidine (27.8 Ma [*Renne et al.*, 1994]) flux monitors to calculate J-factors and K_2SO_4 and CaF_2 salts to calculate correction factors for interfering neutron reactions. All samples were step-heated in a Ta crucible within a double-vacuum furnace. Most $^{40}\text{Ar}/^{39}\text{Ar}$ isotopic measurements were conducted on a VG 1200S or VG 3600 automated mass spectrometer at UCLA. However, some samples, noted in the tabulated results of argon isotopic analyses (Table A4 in auxiliary material), were analyzed at the New Mexico Bureau of Mines and Mineral Resources. Apparent ages were calculated using conventional decay constants and isotopic abundances. Uncertainties for apparent ages listed in Table A4 and cited in the text are at the 1σ level and do not include uncertainties in J factors or decay constants.

[48] Zircons were mounted in epoxy, polished, and coated with ~400 Å of Au. U-Pb single spot analyses on zircon were obtained using the CAMECA ims 1270 ion microprobe at UCLA. The relative sensitivity factor for U and Pb was obtained using a calibration curve defined by measurement of standard zircon AS-3 (1099.1 ± 0.5 Ma [*Paces and Miller*, 1993]). Analyses were made using a 5–15 nA O^- primary beam focused to a spot of ~20 μm diameter. The sample chamber was flooded with O_2^- at a pressure of 3×10^{-5} torr to enhance the yield of Pb^+ ionization. A mass resolving power of ~6000 was used to distinguish the ^{204}Pb peak from

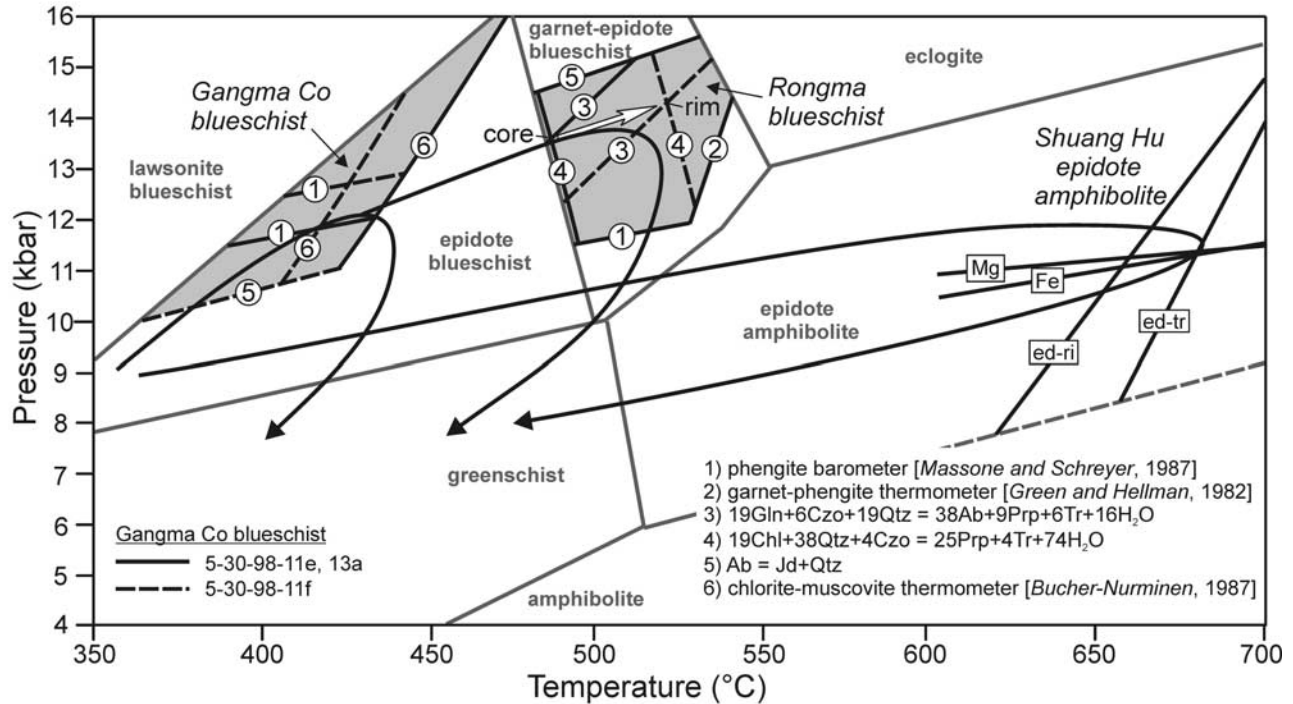


Figure 7. Summary of thermobarometric results for Gangma Co blueschist, Rongma blueschist, and Shuang Hu epidote amphibolite. Schematic P-T paths are based on thermobarometric results coupled with observed mineral parageneses and textural relationships. The dark gray metamorphic facies boundaries are from *Evans* [1990], calculated for a theoretical metabasite with mineral compositions similar to those determined for Gangma Co and Rongma blueschists. The dashed boundary between epidote-amphibolite and amphibolite facies is extrapolated from that of *Evans* [1990] at $T \leq 600^\circ\text{C}$. Clinopyroxene from Gangma Co sample 5-30-98-11f was used to calculate the equilibrium: $\text{Ab} = \text{Jd} + \text{Qtz}$; clinopyroxene in samples 5-30-98-11e and 5-30-98-13a were not used because they were found to be complexly zoned with relict igneous cores and metamorphic rims. Phengite barometry and chlorite-muscovite thermometry provide minimum P and maximum T estimates, respectively, because K-feldspar is absent and water is assumed to have an activity of 1.0. Phengite from Rongma blueschist yield Mg numbers [$100 \times \text{Mg}/(\text{Mg} + \text{Fe})$] of ~ 62 , and the equation of *Green and Hellman* [1982] interpolated for basaltic systems with Mg number of 67 was used for garnet-phengite thermometry. The magnesium (Mg) and iron (Fe), and edenite-richterite (ed-ri) and edenite-tremolite (ed-tr), end-member equilibria were used for garnet-hornblende-plagioclase barometry [*Kohn and Spear*, 1990] and hornblende-plagioclase thermometry [*Holland and Blundy*, 1994] of Shuang Hu epidote amphibolite, respectively.

molecular interferences such as $^{176}\text{Hf}^{28}\text{Si}^+$ [*Compston et al.*, 1984]. Unless noted otherwise, analyses were corrected for common Pb using measured ^{204}Pb and an isotopic composition approximated from the Pb evolution model of *Stacey and Kramers* [1975]. Additional details of the U-Pb analytical method have been described by *Quidelleur et al.* [1997]. U-Pb results are presented as concordia plots with 2σ error ellipses; tabulated results are available in auxiliary material (Table A5).

5.2. Shuang Hu Area

[49] $^{40}\text{Ar}/^{39}\text{Ar}$ analyses were conducted on mineral separates from three samples of epidote amphibolites from the Falong detachment footwall (Figures 8a–8c). Amphibole from sample 97-6-9-4a yields a disturbed age spectrum during the initial 40 cumulative% ^{39}Ar released. We interpret the weighted mean age of 207.8 ± 1.1 Ma for the three

heating steps between 1100° and 1350°C as the time when argon began to be quantitatively retained within the amphibole ($\sim 500^\circ\text{C}$ [*McDougall and Harrison*, 1999]). This is slightly older than the total gas white mica age of 202.8 ± 0.7 Ma for an adjacent sample [97-6-9-4b; *Kapp et al.*, 2000]. Biotite and amphibole from sample 97-6-13-3b yield $^{40}\text{Ar}/^{39}\text{Ar}$ age spectra with age gradients of >100 Ma over the first 30 cumulative percent ^{39}Ar released and total gas ages of 209.5 ± 1.0 and 216.5 ± 1.0 Ma, respectively (Figure 8b). Amphibole from sample 97-6-16-4a yields an age spectrum with maximum apparent ages of ~ 220 Ma and a total gas age of 212.7 ± 1.1 Ma.

5.3. Rongma Area

[50] $^{40}\text{Ar}/^{39}\text{Ar}$ analyses were conducted on mineral separates from three samples of Rongma blueschist (Figures 9d–9e). Phengite from samples 5-31-99-1c and

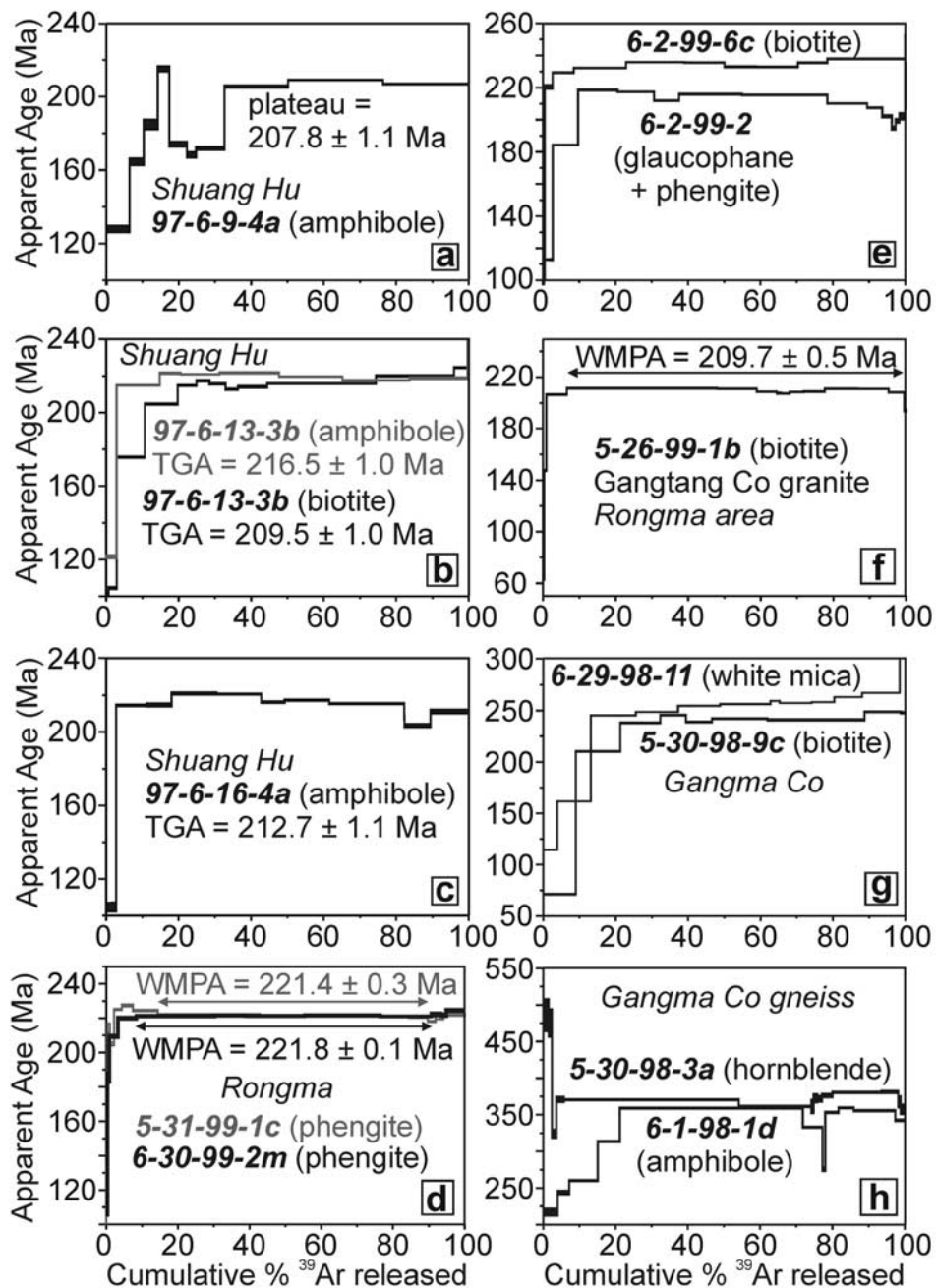


Figure 8. Summary of $^{40}\text{Ar}/^{39}\text{Ar}$ age spectra. WMPA, weighted mean plateau age; TGA, total gas age.

6-30-99-2m yield plateaus with weighted mean ages of 221.4 ± 0.3 Ma and 221.8 ± 0.1 Ma, respectively. Sodic amphibole from sample 6-2-99-2 is overgrown by minor phengite and chlorite and yields an age spectrum that is more disturbed than those provided by the latter samples. However, four of the five steps between 20 and 80 cumulative % ^{39}Ar released yield apparent ages between 220 and 223 Ma. These ages are similar to a published $^{40}\text{Ar}/^{39}\text{Ar}$ total gas age of 222.5 ± 3.7 Ma for crossite from the Rongma area [Li *et al.*, 1995], and are interpreted to

represent the time when Rongma blueschists cooled to below the closure temperature of argon in phengite.

[51] U-Pb single-spot analyses were obtained on 11 zircons separated from the Gangtang Co granite (Foldout 2 and Figure 9a). Seven of nine zircons yield a cluster of concordant ages with a weighted mean $^{206}\text{Pb}^*/^{238}\text{U}$ age of 210 ± 5 Ma (2σ), interpreted to be the age of crystallization. Two spot analyses yielded ages that are discordant and anomalous to that defined by the cluster and were excluded because their UO/U ratios did not lie within the range of the

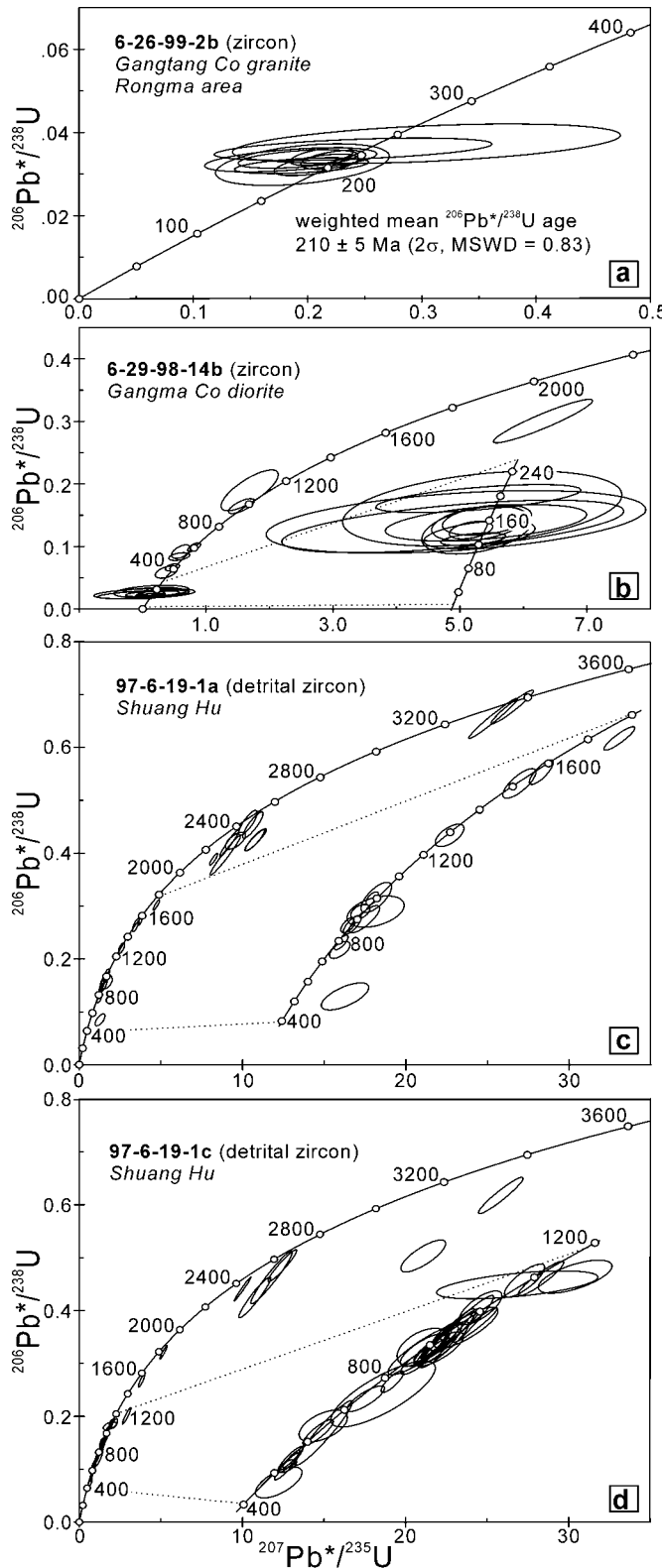


Figure 9. Concordia plots of U-Pb ion microprobe single-spot analyses (error ellipses are 2σ) of zircons from the (a) Gangtang Co granite, (b) Gangma Co diorite, and (c–d) metasediments in the footwall of the Falong detachment, Shuang Hu area.

calibration. Biotite from a different sample of the same granite body (5-20-99-1b) yields a $^{40}\text{Ar}/^{39}\text{Ar}$ age spectrum with a weighted mean age of 209.7 ± 0.5 Ma (Figure 8f).

5.4. Gangma Co Area

[52] Two mica samples from Gangma Co schists yield maximum $^{40}\text{Ar}/^{39}\text{Ar}$ apparent ages between 230 and 270 Ma (Figure 8g). The monotonically rising nature of the age spectra suggests that excess argon may be suspect for explaining variability in maximum apparent ages between samples as well as why they are substantially older than Rongma and Shuang Hu mica ages. Furthermore, it is difficult to evaluate whether the $^{40}\text{Ar}/^{39}\text{Ar}$ results are interpretable in terms of cooling or recrystallization because Gangma Co schists may have equilibrated at temperatures near or below that of argon closure in micas, which can be significantly higher than 350°C at high pressures [e.g., Dahl, 1996].

[53] $^{40}\text{Ar}/^{39}\text{Ar}$ step-heating experiments were conducted on amphibole from two samples of the Gangma Co gneiss. Although significantly disrupted, the flat portions of the age spectra yield ages ranging from 360 to 380 Ma (5-30-98-3a) and 350 to 360 Ma (6-1-98-1d) (Figure 8h). These ages are younger than U-Pb ages of zircons from the Gangma Co gneiss, which range from 419 Ma to 556 Ma [Kapp et al., 2000], and are interpreted to represent the time when the gneiss cooled to below the closure temperature of argon in amphibole.

[54] The diorite that intrudes the Gangma Co gneiss yields two U-Pb zircon age populations that are characterized by different contents of radiogenic Pb (Table A5). The less-radiogenic population yields concordant zircon ages that range from 130 to 200 Ma (Figure 9b). The two oldest zircon analyses in this population plot slightly above a cluster defined by the remaining nine analyses. The latter yield a weighted mean $^{206}\text{Pb}^*/^{238}\text{U}$ age of 139.4 ± 9.1 Ma (2σ), which is interpreted to be the crystallization age. The population of more radiogenic zircons (>95% radiogenic ^{206}Pb) exhibit Paleozoic and older ages, some of which are similar to ages of zircons from the Gangma Co gneiss and detrital zircons from Shuang Hu metasediments (next section).

5.5. U-Pb Detrital Zircon Study of Qiangtang Metasandstones

[55] The provenance of Qiangtang metasediments is constrained by U-Pb ion-microprobe studies on detrital zircons separated from two metasandstones from the Falong detachment footwall (samples 97-6-19-1a and 97-6-19-1c; Foldout 1). Results for 66 spot analyses on 54 detrital zircons from the two samples are shown in Table A5 and as concordia plots in Figures 9c–9d. The ages provided by the two samples are broadly similar, and their combination is taken to represent a preliminary detrital zircon fingerprint for Qiangtang metasediments. Age populations occur at 500 to 700 Ma ($n = 6$), 800 to 1200 Ma ($n = 31$; with a peak at ~ 950 Ma), and between 2.35 and 2.75 Ga ($n = 9$) (Figure 10). In addition, six zircons yield ages between 1.3 and 2.0 Ga and two zircons yield ages of ~ 3.4 Ga and ~ 3.5 Ga.

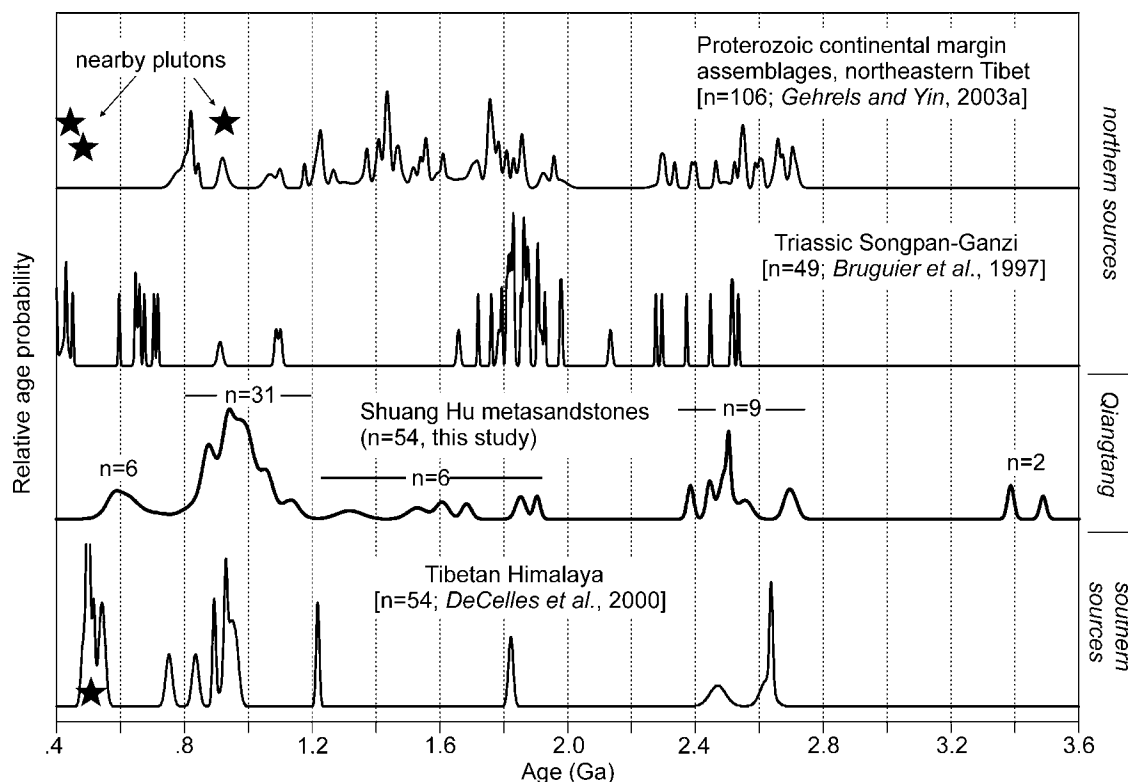


Figure 10. Detrital zircon U-Pb age spectra for Qiangtang metasandstones and other Himalayan-Tibetan terranes. Age spectra are plotted as relative probability curves which were made by fitting normal distributions to the zircon apparent ages and their corresponding 2σ errors, summing them, and then normalizing so that all curves have the same areas. For zircons that are <800 Ma or reversely discordant, $^{206}\text{Pb}^*/^{238}\text{U}$ apparent ages were used. For zircons that are >800 Ma and exhibit normal discordance, $^{207}\text{Pb}^*/^{206}\text{Pb}^*$ apparent ages were used. When multiple spot analyses were obtained on a single zircon (from Qiangtang metasandstones), only the most concordant result was plotted. The stars represent U-Pb zircon ages that have been determined for crystalline rocks in the Himalayan terranes (see references from *DeCelles et al.* [2000]) and northeastern Tibet [*Cowgill et al.*, 2003; *Gehrels et al.*, 2003].

[56] Figure 10 compares the detrital zircon age spectrum for Qiangtang metasandstones to U-Pb ages of detrital zircons within the Songpan-Ganzi flysch complex in eastern Tibet [*Bruguier et al.*, 1997], Proterozoic continental margin assemblages in northeastern Tibet [*Gehrels and Yin*, 2003], and the Tibetan Himalayan sequence south of the Indus suture [*DeCelles et al.*, 2000]. Detrital zircon studies are lacking from the Lhasa and Qiangtang terranes. *Bruguier et al.* [1997] concluded that zircon ages of the Songpan-Ganzi flysch are consistent with it having been derived from sources within the Qinling-Dabie orogen and from the Kunlun arc along the southern margin of the Qaidam terrane. Detrital zircons in Qiangtang metasandstones could have been derived from similar source regions. Most of their ages overlap with those of detrital zircons in the Songpan-Ganzi flysch or Proterozoic continental margin assemblages in northern Tibet. The large population of detrital zircons at ~ 950 Ma, could have been sourced from plutons of this age in northern Tibet [*Gehrels et al.*, 2003]. Possible sources for the 800–1200 Ma zircons include crystalline rocks of these ages in the South China block [*Gao et al.*, 1990; *Jahn et al.*,

1990; *Kröner et al.*, 1993; *Xue et al.*, 1996]. The 2.35 to 2.75 Ga and 3.35 to 3.5 Ga zircons are similar in age to crystalline rocks in the north China block and Dabie Shan orogen [*Liu et al.*, 1985; *Jahn et al.*, 1987; *Kröner et al.*, 1988; *Liu et al.*, 1990, 1992; *Song et al.*, 1996]. The detrital zircon age spectrum for Qiangtang metasandstones also shares many similarities with that for the Tibetan Himalayan sequence. However, a northern provenance is tentatively favored because there are no obvious sources for Early to Middle Archean and ~ 600 Ma zircons in the Himalayan terranes to the south [*DeCelles et al.*, 2000].

6. Discussion

[57] The Qiangtang terrane comprises the highest portion of the Tibetan plateau and exhibits anomalous geophysical properties, enigmatic Cenozoic magmatism, and the largest exposures of metamorphic rocks in the interior of Tibet. Despite its potential to shed insight about the deeper crustal structure of central Tibet, and the mechanisms of burial and exhumation of high-P rocks, the geology of the Qiangtang

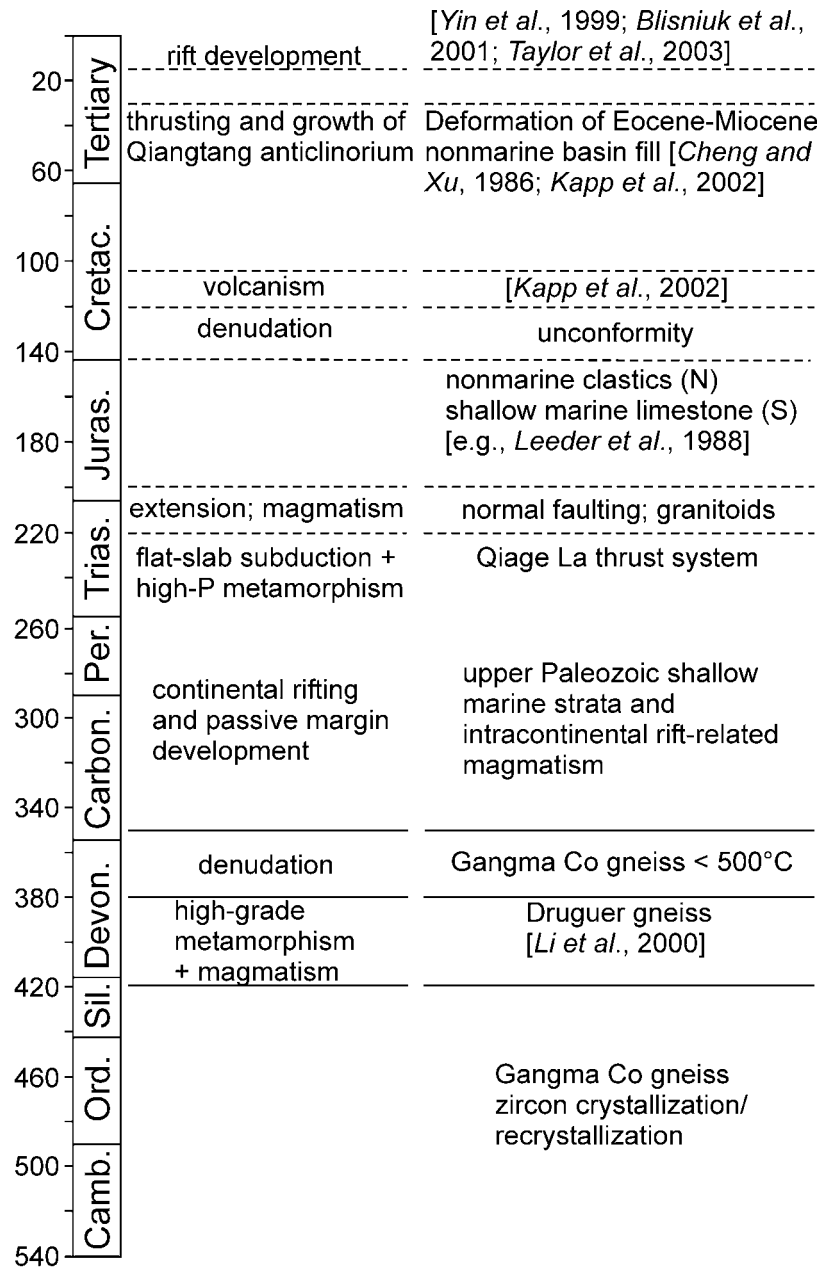


Figure 11. Summary of the Paleozoic–early Mesozoic tectonic evolution of the Qiangtang terrane.

is perhaps the least well studied of the Tibetan terranes. In the following, we present a model for the Paleozoic to early Mesozoic tectonic evolution of the Qiangtang terrane (Figures 11 and 12) that has major implications for the present-day lithospheric structure of central Tibet and accretionary orogenesis in general.

6.1. Paleozoic Basement Evolution and Passive Margin Development

[58] The Gangma Co gneiss is the only exposure of high-grade crystalline rock that has been documented in the Qiangtang terrane. It yielded U-Pb zircon ages that are

similar to those of early Paleozoic gneisses in southern Tibet (Amdo gneiss [Xu *et al.*, 1985]) and crystalline rocks within the Tibetan, Lesser, and Greater Himalaya [e.g., Schärer and Allègre, 1983; Le Fort *et al.*, 1986]. This similarity in zircon ages implies that the Gangma Co gneiss may be a sliver of mafic crystalline basement [Kapp *et al.*, 2000], and that the Qiangtang terrane was contiguous with the Lhasa and Himalayan terranes along the margin of Gondwana during early Paleozoic time.

[59] Upper amphibolite-facies metamorphism of the Gangma Co gneiss occurred prior to 380–350 Ma, the time interval when the gneiss is interpreted to have cooled to below ~500°C. The spread of zircon ages from 556 Ma to

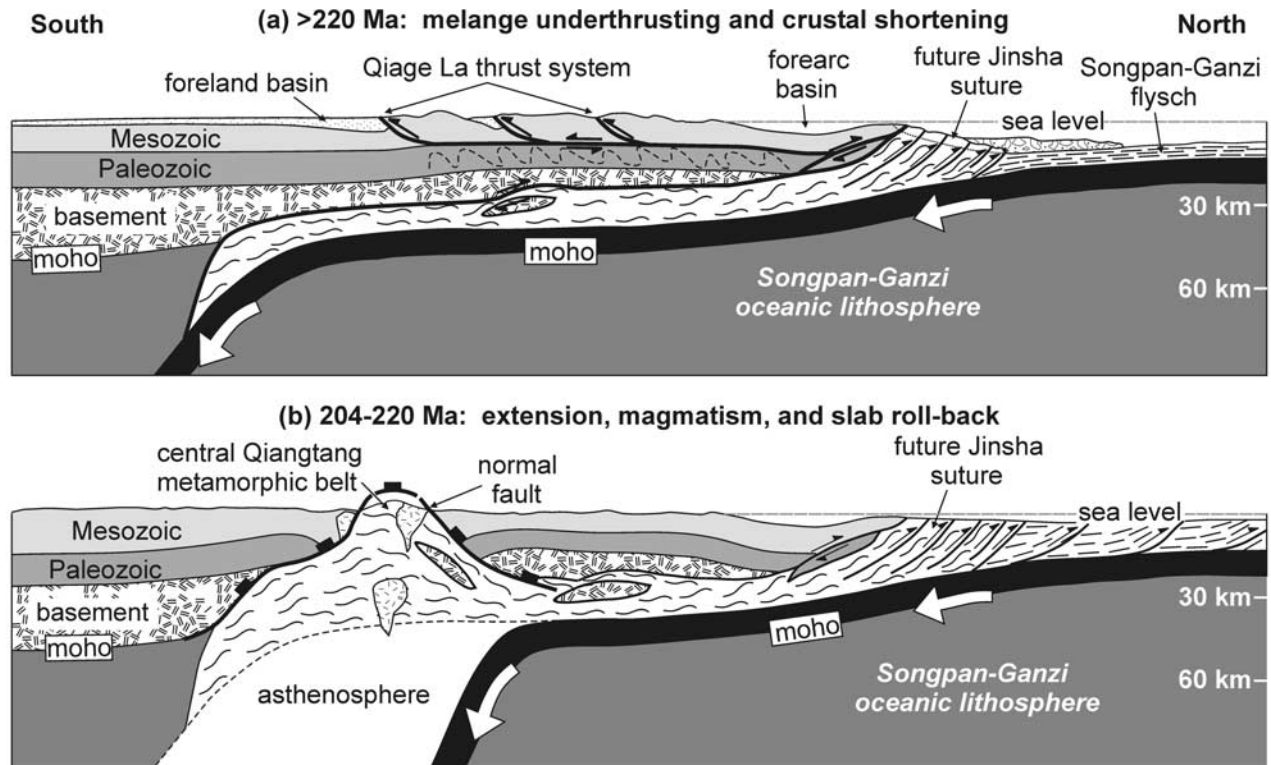


Figure 12. Two-stage model for the early Mesozoic tectonic evolution of central Qiangtang metamorphic rocks that elaborates on the melange underthrusting model of *Kapp et al.* [2000] and *Kapp* [2001]. (a) Melange underthrust southward beneath the Qiangtang continental margin during Triassic low-angle oceanic subduction along the Jinsha suture. The Qiage La thrust system accommodated upper crustal shortening during this time. (b) Exhumation of underthrust melange to upper crustal levels by Late Triassic–Early Jurassic normal faulting, coeval with ongoing subduction. Extension and magmatism may have been initiated by rollback of the subducting oceanic lithosphere. This model predicts that the northern Qiangtang continental mantle was tectonically removed during early Mesozoic time and that the present-day deeper crust of the northern Qiangtang terrane includes large volumes of underthrust early Mesozoic melange.

419 Ma [*Kapp et al.*, 2000] may be a consequence of Pb-loss or recrystallization during middle Paleozoic high-grade metamorphism. A U-Pb zircon age of 384.4 ± 7.4 Ma has been reported for a two-mica-bearing orthogneiss from central Qiangtang (Duguer gneiss [*Li et al.*, 2000]), indicating that high-grade metamorphism may have been associated with magmatism. Regional middle Paleozoic orogenesis could explain why strata older than Middle Devonian are not present in the Qiangtang [*Cheng and Xu*, 1986].

[60] Following middle Paleozoic metamorphism, we infer that Qiangtang basement was nonconformably overlain by Carboniferous-Permian shallow-marine strata. Geochemical signatures of late Paleozoic mafic sills and volcanic rocks in the Qiangtang terrane are characteristic of intracontinental rift-related magmatism [*Zhang et al.*, 1985; *Wang et al.*, 1987; *Pearce and Mei*, 1988; *Li et al.*, 1995; *Deng et al.*, 1996a]. We interpret late Paleozoic rift-related magmatism and deposition of shelf strata to be related to continental breakup and development of a passive margin. The Kunlun terrane to the north exhibits a similar tectonic evolution of

middle Paleozoic orogenesis followed by late Paleozoic passive margin development [*Yin and Harrison*, 2000]. A possible tectonic history is that the Qiangtang terrane collided with the Kunlun terrane during Devonian time, and then subsequently rifted apart during the late Paleozoic to open the Paleo-Tethys Ocean between them [*Cowgill and Kapp*, 2001; *Kapp and Cowgill*, 2001].

6.2. Composition of the CQMB

[61] In the three areas studied, the CQMB is characterized by a matrix of strongly schistose or transposed mafic and metasedimentary rocks that surround lesser-deformed, but variably metamorphosed, blocks of metabasites and sedimentary rocks. This juxtaposition of rocks of variable lithology, deformation, and metamorphic grade is characteristic of accretionary melanges formed in subduction complexes at convergent-plate margins [e.g., *Cloos*, 1982]. The presence of metabasite, metagraywacke, chert, and minor ultramafic material within Qiangtang melange is consistent with it having been derived from fragments of,

and sediments deposited on, oceanic lithosphere. Our detrital zircon study suggests that Qiangtang metasandstones could have been derived from terranes that were north of the Paleo-Tethys Ocean. However, additional work is necessary to characterize detrital zircon signatures of the Tibetan terranes and to evaluate whether sources for ~ 3.4 and ~ 3.5 Ga zircons are unique to terranes north of the Jinsha suture. The CQMB also includes lithologies that are similar to those observed within structurally overlying Carboniferous-Triassic strata, raising the possibility that portions of Qiangtang continental shelf strata were tectonically incorporated by subduction erosion into the melange.

6.3. Melange Metamorphism During Low-Angle Oceanic Subduction (Figure 12a)

[62] It is debated whether Qiangtang melange was (1) thrust beneath the Qiangtang continental margin by ~ 200 km during southward low-angle subduction of oceanic lithosphere along the Jinsha suture [Kapp *et al.*, 2000], or (2) subducted and then exhumed in situ [e.g., Li *et al.*, 1995; Zhang, 2001]. These models make distinct predictions regarding the metamorphic history of the CQMB. Melange that was underthrust beneath a continental margin by flat subduction would be expected to record similar and relatively high pressures of equilibration over a large range of temperatures (see thermal structure of Gutscher *et al.* [2000]). Furthermore, maximum pressures of equilibration should be equal to or greater than that resulting from the thickness of the overlying continental crust \pm mantle. In contrast, the matrix to melange that was subducted and then exhumed closer to the trench should record a large range in pressure at similar and relatively low temperatures characteristic of typical subduction zones (generally $< 350^\circ\text{C}$ at 10 kbar) [Peacock, 1996].

[63] Our petrologic results are consistent with metamorphism of the CQMB within a relatively warm subduction channel beneath a continental margin. Qiangtang melange equilibrated at $P > 10$ kbar at the three widely separated localities studied, and includes rocks that were subducted to ~ 50 km (~ 14 kbar). Whereas pressure estimates remain high, peak temperatures of equilibration decrease systematically from east to west, being $\sim 660^\circ\text{C}$ near Shuang Hu, $\sim 500^\circ\text{C}$ near Rongma, and $\sim 425^\circ\text{C}$ near Gangma Co (Figure 7). Regional differences in observed mineral parageneses (Table A1) and amphibole compositions [Kapp *et al.*, 2000], and deformation fabrics in melange (strongly mylonitized near Shuang Hu versus weak/no stretching lineation near Gangma Co), suggest that this westward decrease in temperature is characteristic of the entire CQMB. The mineral parageneses, mineral compositions, and P-T estimates of the CQMB are strikingly similar to those of the Pelona-Orocopia-Rand schists of southern California [e.g., Jacobson *et al.*, 1988], which were thrust beneath the western North American continental margin during Late Cretaceous–early Tertiary low-angle oceanic subduction [e.g., Yeats, 1968; Burchfiel and Davis, 1981].

[64] Low-angle subduction is consistent with the absence of a well-developed Triassic magmatic arc in central Tibet. Low-angle oceanic subduction may have been contemporaneous with upper crustal shortening, as indicated by the presence of the Late Triassic Qiage La thrust system in the Shuang Hu area. The Gangma Co gneiss may represent basement that was tectonically eroded from the base of the Qiangtang terrane and incorporated into the melange by subduction erosion [Kapp *et al.*, 2000]. The abundance of continental materials of inferred Qiangtang affinity and the scarcity of ultramafic rocks within Qiangtang melange may suggest that it was thrust directly beneath continental crust as opposed to a mantle wedge. Therefore, pressure estimates for Qiangtang melange may indicate a crustal thickness for central Tibet of > 35 km during Late Triassic time. This is consistent with the presence of nonmarine strata of this age in central Tibet [Cheng and Xu, 1986; Leeder *et al.*, 1988; Yin *et al.*, 1988].

[65] Qiangtang melange was exhumed in an intracontinental setting from depths of > 35 km to upper crustal levels by Late Triassic–Early Jurassic normal faulting. In the Shuang Hu area, amphibole total gas $^{40}\text{Ar}/^{39}\text{Ar}$ ages are slightly older than mica total gas ages (by 4 to 7 Ma) within the same sample (97-6-13-3b) or same locality (97-6-9-4a and 97-6-9-4b), and suggest rapid cooling of footwall schists during the time interval over which the Falong detachment must have slipped (between 220 and 204 Ma [Kapp *et al.*, 2000]). Thermobarometric results on a sample of mylonitized epidote amphibolite suggest that the Falong detachment shear zone was active at ~ 11 kbar, and therefore likely cut through the entire crust. In the Rongma area, high-P metamorphism must be younger than Late Triassic radiolarian fossils that have been identified in cherts within the melange [Deng *et al.*, 1996a]. Rongma melange cooled to below the closure temperature for argon in phengite by ~ 222 Ma, and must have been at upper crustal levels prior to intrusion of the ~ 210 Ma Gangtang Co granite. This cooling was likely a consequence of footwall exhumation during slip along the Rongma detachment, which must be younger than the Permian strata it cuts. Portions of the CQMB were at the Earth's surface by Late Triassic time, as indicated by the presence of metamorphic clasts within Upper Triassic sandstones [Xia *et al.*, 2001].

6.4. Rapid Melange Exhumation by Crustal-Scale Normal Faulting (Figure 12b)

[66] The presence of granitoids that both postdate fabric formation in the detachment footwalls (~ 210 Ma Gangtang Co granite) and predate cessation of detachment faulting (~ 220 Ma Shuang Hu granite [Kapp *et al.*, 2000]), suggest that extension may have occurred during ongoing oceanic subduction. A heat source for magmatism and a mechanism to initiate extension may have been provided by rollback of the subducting oceanic lithosphere (Figure 12b). Slab rollback may have been initiated by a decrease in convergence rate during final closure of the Songpan-Ganzi Ocean and initial collision with the Eurasian margin. Detachment faulting in the Shuang Hu and Rongma areas was directed top-to-the-ESE, suggesting that a lateral plate boundary condition may have played an important role in exhumation. The tectonic setting envisioned is similar to that of the Mediterranean region during Oligo-Miocene time, where high-P

rocks were exhumed by low-angle normal faults [e.g., *Lister et al.*, 1984] above retreating oceanic slabs, with slab retreat possibly having been initiated by plate motion reorganization due to Africa-Eurasia collision [*Jolivet and Faccenna*, 2000]. Vertical extrusion of melange may also have been aided by the crustal density inversion that resulted when the melange underthrust higher-density, mafic crystalline lower crust of the Qiangtang terrane [*Martinez et al.*, 2001].

6.5. Implications for Lithospheric Structure and Cenozoic Tectonism of Central Tibet

[67] Cross sections across Qiangtang metamorphic core complexes suggest that melange is much more widespread at depth (Foldouts 1 and 3; Figure 6). The melange underthrusting model predicts that large volumes of early Mesozoic melange may comprise the present-day deeper crust of northern Qiangtang. It was inferred by *Kapp et al.* [2000] that this relatively weak and hydrous material within the deeper crust could (1) have facilitated lithospheric partial melting, crustal shortening, and lower crustal flow in central Tibet during the Cenozoic Indo-Asian collision, and (2) partly explain the anomalously high crustal Poisson's ratios and zones of low seismic velocities [*Owens and Zandt*, 1997] and widespread Cenozoic magmatism [e.g., *Deng*, 1978; *Turner et al.*, 1996] in this area. Early Mesozoic melange in the deeper crust of central Tibet provides a possible explanation for why lower crustal xenoliths in late Cenozoic Qiangtang volcanic rocks include metasedimentary lithologies [*Deng et al.*, 1996b; *Hacker et al.*, 2000a]. *Hacker et al.* [2000a] calculated seismic wave velocities and Poisson's ratios for the xenoliths and showed that they overlap with those suggested from seismological models [*Owens and Zandt*, 1997; *Mechie et al.*, 1999].

[68] The melange underthrusting model further predicts that the Qiangtang continental mantle lithosphere was removed during early Mesozoic low-angle oceanic subduction. Therefore, it is unlikely that partial melting of autochthonous, ancient continental lithosphere can explain Cenozoic magmatogenesis in central Tibet [e.g., *Turner et al.*, 1996]. Underthrust melange may have experienced H₂O-fluxed melting during early Mesozoic rollback of the oceanic slab (Figure 12). In situ melting of these materials a second time at very high T could produce melts of shoshonitic composition [*Patiño Douce and McCarthy*, 1998; *Hacker et al.*, 2000a], which is characteristic of Cenozoic volcanic rocks in central Tibet [e.g., *Deng*, 1978; *Turner et al.*, 1996]. Alternatively, Cenozoic magmatogenesis may be related to continental subduction beneath central Tibet during the Indo-Asian collision [*Deng*, 1991; *Arnaud et al.*, 1992; *Tapponnier et al.*, 2001].

[69] Our studies suggest that the interior of the central Qiangtang terrane experienced minor denudation since Late Triassic–Early Jurassic exhumation of the CQMB and relatively minor upper-crustal shortening during the Indo-Asian collision (see cross sections in Foldouts 1 and 3; Figure 6b). This implies that the central Tibetan crust may have been significantly thickened by flow or thrusting of crust beneath it. The latter may be expressed in surface geology by growth of the ~600-km-long and up to 270 km-

wide east plunging Qiangtang anticlinorium above a major midcrustal thrust ramp [*Yin and Harrison*, 2000].

6.6. Implications for Accretionary Orogens and Evolution of Lower Continental Crust

[70] Our studies on the CQMB provide geologic evidence that large volumes of sediment and upper plate rocks can be incorporated into a subduction channel beneath a continental margin [e.g., *von Huene and Scholl*, 1991; *Vannucchi et al.*, 2001]. The widespread exposure of the CQMB (>500-km long and up to 100-km wide) in an intracontinental setting suggests that subducted materials can be incorporated back into the continental crust, and are not necessarily recycled to the mantle [e.g., *von Huene and Scholl*, 1991]. Our model for large-scale translation of melange beneath, and subsequent exhumation within, a continental margin contrasts strongly with traditional models where high-P metamorphism and exhumation of melange occur within an accretionary wedge close to the trench [e.g., *Cloos*, 1982; *Platt*, 1986]. We suggest that large-scale melange underthrusting during flat-slab oceanic subduction, documented previously only in the western North American Cordillera (Pelona-Orocopia-Rand schists [e.g., *Yeats*, 1968; *Burchfiel and Davis*, 1981; *Jacobson et al.*, 1996]), may be more common than presently thought. Belts of oceanic fragments, flysch, and melange are widespread in Turkey and comprise more than one third of the exposed geology in central Asia. These belts are commonly interpreted to represent in situ suture zones separating distinct micro-continents or arcs [*Hsü et al.*, 1995; *Sengör and Natal'in*, 1996] and have been used to highlight the important role of accretionary complexes in the evolution of continental crust [*Sengör and Okuroğullari*, 1991]. The possibility that some of these belts may represent materials that were underthrust beneath, and subsequently exhumed within, continental interiors would have major implications for paleotectonic reconstructions, the age, composition, and structure of the lower continental crust, and magmatogenesis subsequent to ocean closure.

7. Conclusions

[71] Metamorphic rocks in the central Qiangtang terrane consist of epidote-blueschist-bearing tectonic melange. They were subducted to pressures >10 kbar shortly prior to being exhumed to upper crustal levels in an intracontinental setting by Late Triassic–Early Jurassic crustal-scale normal faults. From east to west, the melange equilibrated at progressively lower temperatures (from ~660°C to ~425°C). Thermobarometric and U-Pb detrital zircon studies are compatible with the melange having underthrust the Qiangtang terrane during southward low-angle oceanic subduction along the Jinsha suture during early Mesozoic time. Mafic crystalline basement exposed within the central Qiangtang crystallized during the early Paleozoic, underwent high-grade metamorphism during the middle Paleozoic, and may have been tectonically incorporated into melange by subduction erosion. The presence of extensive, high-P, early Mesozoic melange in central Tibet, structurally beneath upper Paleozoic and Triassic continental margin strata, provides strong

evidence for significant N-S variations in the present-day composition and structure of the Tibetan crust. Furthermore, it suggests that the process of large-scale translation of melange beneath a continental margin may play a larger role in the evolution of accretionary orogens and lower continental crust than previously thought.

[72] **Acknowledgments.** This research was supported by the U.S. National Science Foundation grant (EAR-98-05340) awarded to A. Yin and

T. M. Harrison, and Geological Society of America and American Association of Petroleum Geologists student grants awarded to P. Kapp. We thank J. D'Andrea, M. Murphy, M. Spurlin, Y. Zhou, X.-G. Deng, and C.-M. Wu for their assistance in the field. G. Gehrels provided a program for calculating relative age probability curves, and K. Ludwig provided the program Isoplot for plotting U-Pb concordia diagrams. We thank F. Kyte for assistance with the electron microprobe analyses and M. Grove and M. Heizler for assistance with $^{40}\text{Ar}/^{39}\text{Ar}$ data collection. This manuscript benefited from discussions with M. Murphy, C. Jacobson, and E. Cowgill, comments by P. Bird and B. Wernicke, and formal reviews by D. Cowan and P. Crowley.

References

- Allègre, C. J., et al., Structure and evolution of the Himalaya-Tibet orogenic belt, *Nature*, 307, 17–22, 1984.
- Arnaud, N. O., P. Vidal, P. Tapponnier, P. Matte, and W. M. Deng, The high K_2O volcanism of northwestern Tibet: Geochemistry and tectonic implications, *Earth Planet. Sci. Lett.*, 111, 351–367, 1992.
- Bao, P. S., X. C. Xiao, J. Wang, C. Li, and K. Hu, The blueschist belt in the Shuanghu region, central-northern Tibet, and its tectonic implications, *Acta Geol. Sin.*, 73, 302–314, 1999.
- Berman, R. G., Internally-consistent thermodynamic data for stoichiometric minerals in the system $\text{Na}_2\text{O}-\text{K}_2\text{O}-\text{CaO}-\text{MgO}-\text{FeO}-\text{Fe}_2\text{O}_3-\text{Al}_2\text{O}_3-\text{SiO}_2-\text{TiO}_2-\text{H}_2\text{O}-\text{CO}_2$, *J. Petrol.*, 29, 445–522, 1988.
- Berman, R. G., Thermobarometry using multiequilibrium calculations: A new technique with petrologic applications, *Can. Mineral.*, 29, 833–855, 1991.
- Bruguier, O., J. R. Lancelot, and J. Malavieille, U-Pb dating on single detrital zircon grains from the Triassic Sonpan-Ganze flysch (Central China): Provenance and tectonic correlations, *Earth Planet. Sci. Lett.*, 152, 217–231, 1997.
- Bucher-Nurminen, K., A recalibration of the chlorite-biotite-muscovite geobarometer, *Contrib. Mineral. Petrol.*, 96, 519–522, 1987.
- Burchfiel, B. C., and G. A. Davis, Mojave Desert and environs, in *The Geotectonic Development of California (Rubey Vol. 1)*, edited by W. G. Ernst, pp. 217–252, Prentice-Hall, Old Tappan, N. J., 1981.
- Burchfiel, B. C., P. Molnar, Z. Zhao, K. U. Liang, S. Wang, M. Huang, and J. Sutter, Geology of the Ulugh Muztagh area, northern Tibet, *Earth Planet. Sci. Lett.*, 94, 57–70, 1989.
- Burchfiel, B. C., Z. Chan, Y. Liu, and L. H. Royden, Tectonics of the Longmen Shan and adjacent regions, central China, *Int. Geol. Rev.*, 37, 661–735, 1995.
- Chang, C.-F., and S.-L. Zheng, Tectonic features of the Mount Jolmu Lungma region in southern Tibet, China (in Chinese), *Sci. Geol. Sin.*, 1 (1–12), 1973.
- Chen, B., and G. Xie, Evolution of the Tethys in Yunnan and Tibet, *J. Southeast Asian Earth Sci.*, 9, 349–354, 1994.
- Cheng, J., and G. Xu, Geologic map of the Gaize region with report, 369 pp., Tibetan Bur. of Geol. and Miner. Resour., Chengdu, People's Republic of China, 1986.
- Cheng, J., and G. Xu, Geologic map of the Ritu region with report, 598 pp., Tibetan Bur. of Geol. and Miner. Resour., Chengdu, People's Republic of China, 1987.
- Cloos, M., Flow melanges: Numerical modeling and geologic constraints on their origin in the Franciscan subduction complex, California, *Geol. Soc. Am. Bull.*, 93, 330–345, 1982.
- Compston, W., I. S. Williams, and C. Meyer, U-Pb Geochronology of zircons from Lunar Breccia 73,217 using a sensitive high mass-resolution ion microprobe, *J. Geophys. Res.*, 89, Suppl., 525–534, 1984.
- Cowgill, E., and P. Kapp, Did Tarim (+North China) collide with Qiangtang (+South China) in both the Devonian and the Triassic?, *Geol. Soc. Am. Abstr. Programs*, 33, 42, 2001.
- Cowgill, E., A. Yin, T. M. Harrison, and X.-F. Wang, Reconstruction of the Altyn Tagh fault based on U-Pb geochronology: Role of back thrusts, mantle sutures, and heterogeneous crustal strength in forming the Tibetan Plateau, *J. Geophys. Res.*, 108, doi:10.1029/2002JB002080, in press, 2003.
- Dahl, P. S., The crystal-chemical basis for Ar retention in micas: Inferences from interlayer partitioning and implications for geochronology, *Contrib. Mineral. Petrol.*, 123, 22–39, 1996.
- DeCelles, P. G., G. E. Gehrels, J. Quade, B. LaReau, and M. Spurlin, Tectonic implications of U-Pb zircon ages of the Himalayan orogenic belt in Nepal, *Science*, 288, 497–499, 2000.
- Deng, W., A preliminary study on the petrology and petrochemistry of the Quaternary volcanic rocks of northern Tibet autonomous region (in Chinese), *Acta Geol. Sin.*, 52, 148–162, 1978.
- Deng, W., Cenozoic volcanism and intraplate subduction at the northern margin of the Tibetan Plateau, *Chin. J. Geochem.*, 10, 140–152, 1991.
- Deng, W., J. Yin, and Z. Guo, Basic-ultrabasic and volcanic rocks in Chagbu-Shuanghu area of northern Xizang (Tibet), China, *Sci. China Ser. D*, 359–368, 1996a.
- Deng, W., X. Zheng, and Y. Matsumoto, Petrological characteristics and ages of Cenozoic volcanic rocks from the Hoh Xil Mountains, Qinghai, *Acta Petrol. Miner.*, 15, 289–298, 1996b.
- Deng, X., L. Ding, and Y. Zhou, Petrology and $^{40}\text{Ar}/^{39}\text{Ar}$ isotopic ages of blueschists in Gangmar, central Qiangtang, northern Tibet, *Chin. Sci. Bull.*, 46, 423–427, 2001.
- Dewey, J. F., and K. C. A. Burke, Tibetan, Variscan and Precambrian basement reactivation: Products of continental collision, *J. Geol.*, 81, 683–692, 1973.
- Dewey, J. F., R. M. Shackleton, C. Chang, and S. Yiyin, The tectonic evolution of the Tibetan Plateau, *Philos. Trans. R. Soc. London, Ser. A*, 327, 379–413, 1988.
- Evans, B. W., Phase relations of epidote-blueschists, *Lithos*, 25, 3–23, 1990.
- Fan, Y. N., A division of zoogeographical provinces by Permo-Carboniferous corals in Xizang, China, *Contrib. Geol. Qinghai-Xizang Plateau*, 16, 105–112, 1985.
- Fan, Y. N., *The Carboniferous System in Xizang*, 128 pp., Chongqing Publ. House, Chongqing, People's Republic of China, 1988.
- Gao, S., B. Zhang, and Z. Li, Geochemical evidence for Proterozoic continental arc and continental-margin rift magmatism along the northern margin of the Yangtze Craton, South China, *Precambrian Res.*, 47, 205–221, 1990.
- Gehrels, G. E., and A. Yin, Detrital zircon geochronology of the northeastern Tibetan Plateau, *Geol. Soc. Am. Bull.*, in press, 2003.
- Gehrels, G. E., A. Yin, and X.-F. Wang, Magmatic history of the northeastern Tibetan Plateau, *J. Geophys. Res.*, 108, doi:10.1029/2002JB001876, in press, 2003.
- Girardeau, J., J. Marcoux, C. J. Allegre, J. P. Bassoullet, T. Youking, X. Xuchang, Z. Yougong, and W. Xibin, Tectonic environment and geodynamic significance of the Neo-Cimmerian Donqiao ophiolite, Bangong-Nujiang suture zone, Tibet, *Nature*, 307, 27–31, 1984.
- Green, T. H., and P. L. Hellman, Fe-Mg partitioning between coexisting garnet and phengite at high pressure, and comments on a garnet-phengite thermometer, *Lithos*, 17, 253–266, 1982.
- Gutscher, M.-A., R. Maury, J.-P. Eissen, and E. Bourdon, Can slab melting be caused by flat subduction?, *Geology*, 28, 535–538, 2000.
- Hacker, B. R., E. Gnos, L. Ratschbacher, M. Grove, M. McWilliams, S. V. Sobolev, J. Wan, and W. Zhenhan, Hot and dry deep crustal xenoliths from Tibet, *Science*, 287, 2463–2466, 2000a.
- Hacker, B. R., L. Ratschbacher, L. Webb, O. McWilliams, T. Ireland, A. Calvert, S. Dong, H.-R. Wenk, and D. Chateigner, Exhumation of ultrahigh-pressure continental crust in east central China: Late Triassic-Early Jurassic tectonic unroofing, *J. Geophys. Res.*, 105, 13,339–13,364, 2000b.
- Hedin, S. A., *Central Asia Atlas by Sven Hedin*, Statens Etnografiska Museum, Stockholm, 1966.
- Hennig, A., Zur Petrographie und geologie von Südwest Tibet, in *Southern Tibet*, vol. 5, edited by S. Hedin, 220 pp., Norstedt, Stockholm, 1915.
- Holland, T., and J. Blundy, Non-ideal interactions in calcic amphiboles and their bearing on amphibole-plagioclase thermometry, *Contrib. Mineral. Petrol.*, 116, 433–447, 1994.
- Hou, L., D. Luo, D. Fu, S. Hu, and K. Li, *Triassic Sedimentary-Tectonic Evolution in Western Sichuan and Eastern Xizang Region*, 220 pp., Geol. Publ. House, Beijing, 1991.
- Hsü, K. J., P. Guitang, and A. M. C. Sengör, Tectonic evolution of the Tibetan Plateau: A working hypothesis based on the Archipelago model of orogenesis, *Int. Geol. Rev.*, 37, 473–508, 1995.
- Jacobson, C. E., M. R. Dawson, and C. E. Postlethwaite, Structure, metamorphism, and tectonic significance of the Pelona, Orocofia, and Rand schists, southern California, in *Metamorphism and Crustal Evolution in the Western United States*, edited by W. G. Ernst, pp. 976–997, Prentice-Hall, Old Tappan, N. J., 1988.
- Jacobson, C. E., F. R. Oyarzabal, and G. B. Haxel, Subduction and exhumation of the Pelona-Orocofia-Rand Schists, southern California, *Geology*, 24, 547–550, 1996.
- Jahn, B. M., B. Auvray, J. Cornichet, Y. L. Bai, Q. H. Shen, and D. Y. Liu, 3.5 Ga old amphibolites from eastern Hebei Province, China: Field occurrence, petrography, Sm-Nd isochron age and REE geochemistry, *Precambrian Res.*, 34, 311–346, 1987.
- Jahn, B. M., X. H. Zhou, and J. L. Li, Formation and tectonic evolution of Southeastern China and Taiwan: Isotopic and geochemical constraints, *Tectonophysics*, 183, 145–160, 1990.

- Jolivet, L., and C. Faccenna, Mediterranean extension and the Africa-Eurasia collision, *Tectonics*, 19, 1095–1106, 2000.
- Kapp, P., Blueschist-bearing metamorphic core complexes in the Qiangtang block reveal deep crustal structure of northern Tibet: Reply, *Geology*, 29, 91, 2001.
- Kapp, P., and E. Cowgill, Does the Paleozoic tectonic history of Qiangtang record the formation and break-up of a Devonian supercontinent?, *Geol. Soc. Am. Abstr. Programs*, 33, 42, 2001.
- Kapp, P., A. Yin, C. E. Manning, M. Murphy, T. M. Harrison, M. Spurlin, L. Ding, X.-G. Deng, and C.-M. Wu, Blueschist-bearing metamorphic core complexes in the Qiangtang block reveal deep crustal structure of northern Tibet, *Geology*, 28, 19–22, 2000.
- Kapp, P., A. Yin, T. M. Harrison, and L. Ding, Cretaceous-Tertiary deformation history of central Tibet, *Geol. Soc. Am. Abstr. Programs*, 34, 487, 2002.
- Kidd, W. S. F., Y. Pan, C. Chang, M. P. Coward, J. F. Dewey, F. R. S. A. Gansser, P. Molnar, R. M. Shackleton, and Y. Sun, Geological mapping of the 1985 Chinese-British Tibetan (Xizang-Qinghai) Plateau Geotraverse route, *Philos. Trans. R. Soc. London, Ser. A*, 327, 287–305, 1988.
- Kohn, M. J., and F. S. Spear, Two new geobarometers for garnet amphibolites, with applications to south-eastern Vermont, *Am. Mineral.*, 75, 89–96, 1990.
- Kretz, R., Symbols for rock-forming minerals, *Am. Mineral.*, 68, 277–279, 1983.
- Kröner, A., W. Compston, G. Zhang, A. Guo, and W. Todt, Age and tectonic setting of Late Archean greenstone-gneiss terrain in Henan Province, China, as revealed by single-grain zircon dating, *Geology*, 16, 211–215, 1988.
- Kröner, A., G. W. Zhang, and Y. Sun, Granulites in the Tongbai area, Qinling belt, China: Geochemistry, petrology, single zircon geochronology, and implications for the tectonic evolution of eastern Asia, *Tectonics*, 12, 245–255, 1993.
- Leeder, M. R., A. B. Smith, and Y. Jixiang, Sedimentology and palaeoenvironmental evolution of the 1985 Lhasa to Golmud geotraverse, *Philos. Trans. R. Soc. London, Ser. A*, 327, 107–143, 1988.
- Le Fort, P., F. Debon, A. Pecher, J. Sonet, and P. Vidal, The 500 Ma magmatic event in the Alpine Southern Asia: A thermal episode at Gondwana scale, *Sci. Terre Mem.*, 47, 191–200, 1986.
- Li, C., The Longmu Co-Shuanghu-Lancangjiang Suture as the northern boundary of the Gandwanaland in the Carboniferous and Permian, *Bull. Changchun Coll. Geol. Sci.*, 17, 155–166, 1987.
- Li, C., and A. Zheng, Paleozoic stratigraphy in the Qiangtang region of Tibet: Relations of the Gondwana and Yangtze continents and ocean closure near the end of the Carboniferous, *Int. Geol. Rev.*, 35, 797–804, 1993.
- Li, C., C. Liren, H. Ke, Y. Zengrong, and H. Yurong, Study on the paleo-Tethys suture zone of Lungmu Co-Shuanghu, Tibet, 131 pp., Geol. Publ. House, Beijing, 1995.
- Li, C., T. Wang, D. Yang, Z. He, and Y. Ren, Study on the isotopic chronology and tectonic significance of Duguer granitic gneiss in central Qiangtang, Tibet, in *15th Himalaya-Karakorum-Tibet Workshop*, vol. 7, pp. 182–183, Earth Sci. Frontiers, China Univ. of Geosci., Beijing, Chengdu, China, 2000.
- Lister, G. S., G. Banga, and A. Feenstra, Metamorphic core complexes of Cordilleran type in the Cyclades, Aegean Sea, Greece, *Geology*, 12, 221–225, 1984.
- Liu, D., R. W. Page, W. Compston, and J. Wu, U-Pb zircon geochronology of Late Archean metamorphic rocks in the Taihangshan-Wutaishan area, North China, *Precambrian Res.*, 27, 85–109, 1985.
- Liu, D. Y., Q. H. Shen, Z. Q. Zhang, B. M. Jahn, and B. Auvray, Archean crustal evolution in China: U-Pb geochronology of the Qianxi Complex, *Precambrian Res.*, 48, 223–244, 1990.
- Liu, D. Y., A. P. Nutman, W. Compston, J. S. Wu, and Q. H. Shen, Remnants of >3800 Ma crust in the Chinese part of the Sino-Korean craton, *Geology*, 20, 339–342, 1992.
- Liu, Z. Q., Geologic map of the Qinghai-Xizang Plateau and its neighboring regions (scale at 1:1,500,000), Chengdu Inst. of Geol. and Miner. Resour., Geol. Publ. House, Beijing, 1988.
- Martinez, F., A. M. Goodliffe, and B. Taylor, Metamorphic core complex formation by density inversion and lower-crust extrusion, *Nature*, 411, 930–934, 2001.
- Massonne, H., and W. Schreyer, Phengite geobarometry based on limiting assemblage with K-feldspar, phlogopite, and quartz, *Contrib. Mineral. Petrol.*, 96, 212–224, 1987.
- Matte, P., P. Tapponnier, N. Arnaud, L. Bourjot, J. P. Avouac, P. Vidal, Q. Liu, Y. Pan, and Y. Wang, Tectonics of Western Tibet, between the Tarim and the Indus, *Earth Planet. Sci. Lett.*, 142, 311–330, 1996.
- McDougall, I., and T. M. Harrison, *Geochronology and Thermochronology by the ⁴⁰Ar/³⁹Ar Method*, 261 pp., Oxford Univ. Press, New York, 1999.
- Mechie, J., L. D. Brown, S. Haines, S. L. Klempner, R. Meissner, K. D. Nelson, W. Zhao, and J. Guo, Crustal structure in central Tibet as derived from wide-angle seismic data, *Eos Trans. AGU*, 8046, Fall Meet. Suppl., F951, 1999.
- Metcalfe, I., Gondwanaland dispersion, Asian accretion and evolution of eastern Tethys, *Aust. J. Earth Sci.*, 43, 605–623, 1996.
- Meyer, B., P. Tapponnier, L. Bourjot, F. Metivier, Y. Gaudemer, G. Peltzer, S. Guo, and Z. Chen, Crustal thickening in Gansu-Qinghai, lithospheric mantle subduction, and oblique, strike-slip controlled growth of the Tibet plateau, *Geophys. J. Int.*, 135, 1–47, 1998.
- Nie, S., A. Yin, D. B. Rowley, and Y. Jin, Exhumation of the Dabie Shan ultra-high pressure rocks and accumulation of the Songpan-Ganzi flysch sequence, central China, *Geology*, 22, 999–1002, 1994.
- Owens, T. J., and G. Zandt, Implications of crustal property variations for models of Tibetan plateau evolution, *Nature*, 387, 37–43, 1997.
- Paces, J. B., and J. D. Miller, Precise U-Pb age of Duluth Complex and related mafic intrusions, northeastern Minnesota: Geochronological insights into physical, petrogenetic, paleomagnetic, and tectonomagmatic processes associated with the 1.1 Ga midcontinent rift system, *J. Geophys. Res.*, 98, 13,997–14,013, 1993.
- Patiño Douce, A. E., and T. C. McCarthy, Melting of crustal rocks during continental collision and subduction, in *Geodynamics and Geochemistry of Ultrahigh-Pressure Rocks*, edited by B. R. Hacker and J. G. Liou, pp. 27–55, Kluwer Acad., Norwell, Mass., 1998.
- Peacock, S. M., Thermal and petrologic structure of subduction zones, in *Subduction: Top to Bottom*, *Geophys. Monogr. Ser.*, vol. 96, edited by G. E. Bebout et al., pp. 119–133, AGU, Washington, D. C., 1996.
- Pearce, J. A., and W. Deng, The ophiolites of the Tibetan Geotraverses, Lhasa to Golmud (1985) and Lhasa to Kathmandu (1986), *Philos. Trans. R. Soc. London, Ser. A*, 327, 215–238, 1988.
- Pearce, J. A., and H. Mei, Volcanic rocks of the 1985 Tibet Geotraverse: Lhasa to Golmud, *Philos. Trans. R. Soc. London, Ser. A*, 327, 169–201, 1988.
- Platt, J. P., Dynamics of orogenic wedges and the uplift of high-pressure metamorphic rocks, *Geol. Soc. Am. Bull.*, 97, 1037–1053, 1986.
- Powell, R., and J. Evans, A new geobarometer for the assemblage biotite-muscovite-chlorite-quartz., *J. Meteorol. Geol.*, 1, 331–336, 1983.
- Quidelleur, X., M. Grove, O. M. Lovera, T. M. Harrison, and A. Yin, Thermal evolution and slip history of the Renbu-Zedong Thrust, southeastern Tibet, *J. Geophys. Res.*, 102, 2659–2679, 1997.
- Rao, R., J. Xu, Y. Chen, and D. Zou, *The Triassic System of the Qinghai-Xizang Plateau*, 239 pp., Geol. Publ. House, Beijing, 1987.
- Renne, P. R., A. L. Deino, R. C. Walter, B. D. Turrin, C. C. Swisher, T. A. Becker, G. H. Curtis, W. D. Sharp, and A. R. Jaouni, Intercalibration of astronomical and radioisotopic time, *Geology*, 22, 783–786, 1994.
- Schärer, U., and C. J. Allègre, The Palung granite (Himalaya); high-resolution U-Pb systematics in zircon and monazite, *Earth Planet. Sci. Lett.*, 63, 423–433, 1983.
- Sengör, A. M. C., and B. A. Natal'in, Paleotectonics of Asia: Fragments of a synthesis, in *The Tectonic Evolution of Asia*, edited by A. Yin and T. M. Harrison, pp. 486–640, Cambridge Univ. Press, New York, 1996.
- Sengör, A. M. C., and A. H. Okuroğullari, The role of accretionary wedges in the growth of continents: Asiatic examples from Argand to plate tectonics, *Ecolgae Geol. Helv.*, 84, 535–597, 1991.
- Sengör, A. M. C., D. Altiner, A. Cin, T. Ustaomer, and K. J. Hsu, Origin and assembly of the Tethyside orogenic collage at the expense of Gondwana Land, *Geol. Soc. Spec. Publ.*, 37, 119–181, 1988.
- Song, B., A. P. Nutman, D. Liu, and J. Wu, 3800 to 2500 Ma crustal evolution in the Anshan area of Lianing Province, northeastern China, *Precambrian Res.*, 78, 79–94, 1996.
- Stacey, J. S., and J. D. Kramers, Approximation of terrestrial lead isotope evolution by a two-stage model, *Earth Planet. Sci. Lett.*, 26, 207–221, 1975.
- Tang, Y., and F. Wang, Primary analysis of the tectonic environment of the ophiolite in Northern Xizang, *Himalayan Geol.*, 2, 99–113, 1984.
- Tapponnier, P., Z. Xu, F. Roger, B. Meyer, N. Arnaud, G. Wittlinger, and J. Yang, Oblique stepwise rise and growth of the Tibet Plateau, *Science*, 294, 1671–1677, 2001.
- Taylor, M., A. Yin, F. J. Ryerson, P. Kapp, and L. Ding, Conjugate strike-slip faulting along the Bangong-Nujiang suture zone accommodates coeval east-west extension and north-south shortening in the interior of the Tibetan Plateau, *Tectonics*, 22, doi:10.1029/2002TC001361, in press, 2003.
- Turner, S., N. Arnaud, J. Liu, N. Rogers, C. Hawkesworth, N. Harris, S. Kelley, P. Van Calsteren, and W. Deng, Post-collision, shoshonitic volcanism on the Tibetan plateau: Implications for convective thinning of the lithosphere and the source of ocean island basalts, *J. Petrol.*, 37, 45–71, 1996.
- Vannucchi, P., D. W. Scholl, M. Meschede, and K. McDougall-Reid, Tectonic erosion and consequent collapse of the Pacific margin of Costa Rica: Combined implications from ODP Leg 170, seismic offshore data, and regional geology of the Nicoya Peninsula, *Tectonics*, 20, 649–668, 2001.
- von Huene, R., and D. W. Scholl, Observations at convergent margins concerning sediment subduction, subduction erosion, and the growth of continental crust, *Rev. Geophys.*, 29, 279–316, 1991.
- Wang, C., C. Hu, and R. Wu, Discovery and geologic significance of the Casang-Cabu rift in northern Xizang, *Bull. Chengdu Coll. Geol. Sci.*, 14, 33–46, 1987.
- Wang, Y.-J., and X.-N. Mu, Upper Carboniferous and Lower Permian strata in the Gondwana-Tethys province in Xizang (Tibet), *Palaeontol. Cathayana*, 1, 411–419, 1983.
- Xia, B. D., C. Li, and H. F. Ye, Blueschist-bearing metamorphic core complexes in the Qiangtang block reveal deep crustal structure of northern Tibet: Comment, *Geology*, 29, 663, 2001.
- Xu, R.-H., U. Schärer, and C. J. Allègre, Magmatism and metamorphism in the Lhasa block (Tibet): A geochronological study, *J. Geol.*, 93, 41–57, 1985.
- Xue, F., A. Kröner, T. Reischmann, and F. Lerch, Palaeozoic pre- and post-collision calc-alkaline magmatism in the Qinling orogenic belt, central China, as documented by zircon ages on granitoid rocks, *J. Geol. Soc. London*, 153, 409–417, 1996.
- Yeats, R. S., Southern California structure, seafloor spreading, and history of the Pacific Basin, *Geol. Soc. Am. Bull.*, 79, 1693–1702, 1968.

- Yin, A., and J. F. Dunn, Structural and stratigraphic development of the Whipple-Chemehuevi detachment fault system, southeastern California: Implications for the geometrical evolution of domal and basinal low-angle normal faults, *Geol. Soc. Am. Bull.*, 104, 659–674, 1992.
- Yin, A., and T. M. Harrison, Geologic evolution of the Himalayan-Tibetan orogen, *Annu. Rev. Earth Planet. Sci.*, 28, 211–280, 2000.
- Yin, A., and S. Nie, A Phanerozoic palinspastic reconstruction of China and its neighboring regions, in *The Tectonic Evolution of Asia*, edited by A. Yin and T. M. Harrison, pp. 442–485, Cambridge Univ. Press, New York, 1996.
- Yin, A., P. A. Kapp, M. A. Murphy, T. M. Harrison, M. Grove, L. Ding, X. Deng, and C. Wu, Significant late Neogene east-west extension in northern Tibet, *Geology*, 27, 787–790, 1999.
- Yin, J., J. Xu, C. Liu, and H. Li, The Tibetan plateau: Regional stratigraphic context and previous work, *Philos. Trans. R. Soc. London, Ser. A.*, 327, 5–52, 1988.
- Zhang, K.-J., Blueschist-bearing metamorphic core complexes in the Qiangtang block reveal deep crustal structure of northern Tibet: Comment, *Geology*, 29, 90, 2001.
- Zhang, M., C. Hu, and R. Wu, Geochemical characteristics and tectonic setting of the Xiangqiong-Casang mafic volcanic belt, *Geol. Res. Qinghai-Xizang Plateau*, 9, 57–68, 1985.
- Zhong, D., *Paleotethyan Orogenic Belts in Yunan and Western Sichuan*, 230 pp., Sci. Publ. House, Beijing, 1998.
- Zhou, D., and S. A. Graham, The Songpan-Ganzi complex of the West Qinling Shan as a Triassic remnant ocean basin, in *The Tectonic Evolution of Asia*, edited by A. Yin and T. M. Harrison, pp. 281–299, Cambridge Univ. Press, New York, 1996.
-
- L. Ding, Institute of Geology and Geophysics, Chinese Academy of Sciences, Beijing 100029, People's Republic of China. (dinglin@mail.igcas.ac.cn)
- T. M. Harrison, C. E. Manning, M. H. Taylor, and A. Yin, Department of Earth and Space Sciences, 3651 Geology Building, University of California, Los Angeles, CA 90095-156702, USA. (mark.harrison@anu.edu.au; manning@ess.ucla.edu; mtaylor@ess.ucla.edu; yin@ess.ucla.edu)
- P. Kapp, Department of Geosciences, University of Arizona, Gould-Simpson Building, Tucson, AZ 85721, USA. (pkapp@geo.arizona.edu)

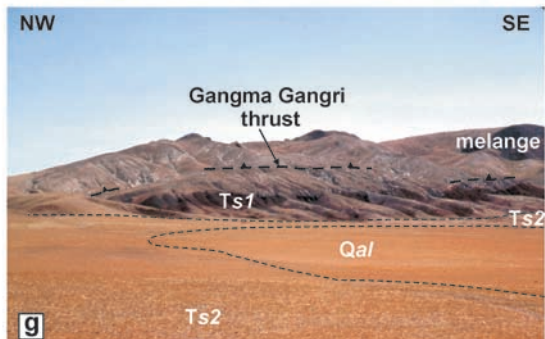
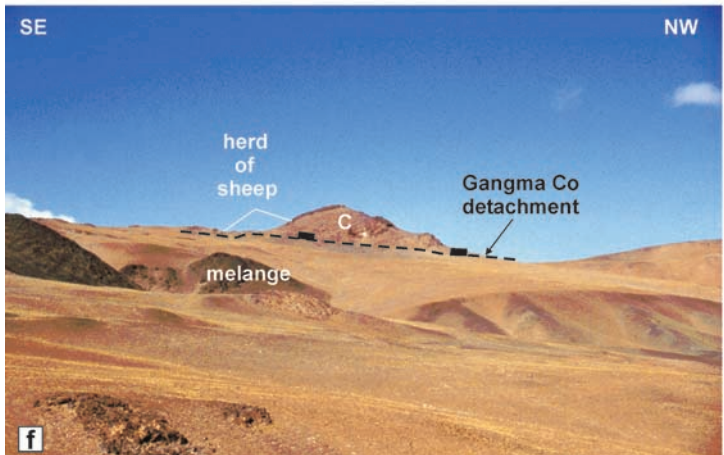
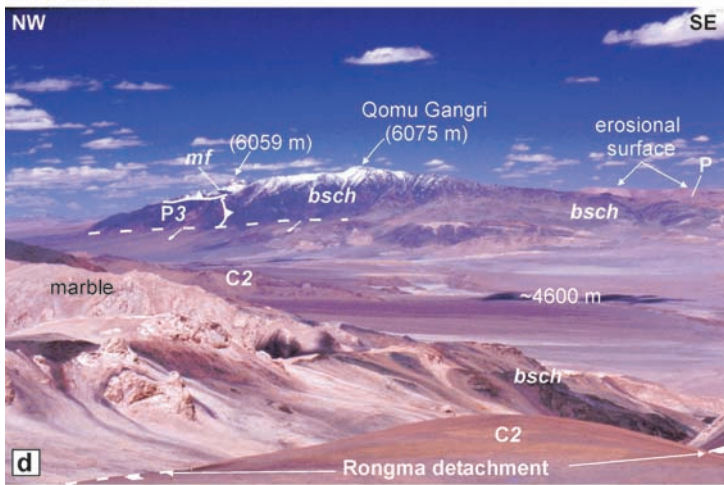
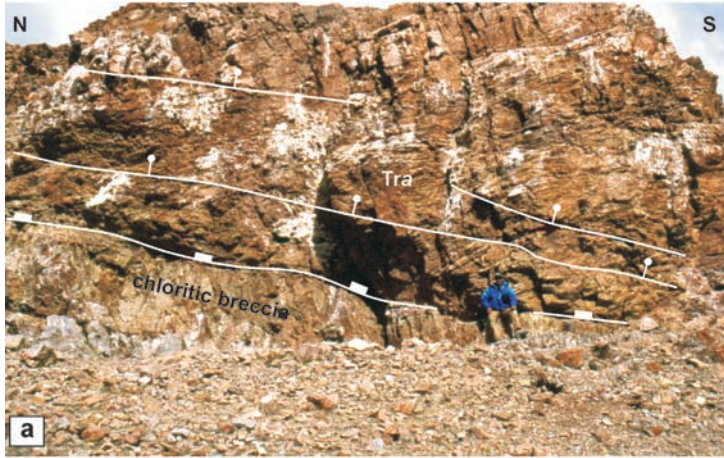


Figure 5. (opposite) (a) View to east at Falong detachment near locality 97-6-13-3 (Foldout 1). Hanging wall normal faults dip into the plane of the photo. (b) View to west at 10–20-m-thick zone of chloritic breccia directly beneath Falong detachment near locality 97-6-9-4 (Foldout 1). It grades structurally below into light-colored mylonitic schists and gneisses. (c) View to north at mylonitic S-C fabrics in the footwall of the Falong detachment which indicate top-to-the-ESE sense-of-shear. (d) View to northeast across Yibug Caka river valley at Qomu Gangri peak in the Rongma area (Foldout 2). In the foreground, the Rongma detachment juxtaposes hanging wall Carboniferous limestone, C2, against footwall blueschist-bearing melange, bsch, with blocks of marble. Abbreviations: P, Permian strata, undivided; P3, Permian mafic volcanic rocks and conglomerates; mf, mafic gabbro. The prominent river valley and elevated erosional surface in background are related to the late Cenozoic Yibug Caka rift system [Taylor *et al.*, 2003]. (e) View to north at locality 5-29-99-1 in the Rongma area (Foldout 2). Several listric normal faults within Carboniferous limestone, C2, root into a low-angle zone of fault breccia and gouge, which characterizes the Rongma detachment. Structurally below is metabasite-bearing melange. (f) View to southwest near locality 98-5-28-1 at the Gangma Co detachment (Foldout 3). Here, it is defined by a low-angle zone of dark fault breccia directly beneath tilted Carboniferous limestone, C, in the hanging wall. Footwall lithologies include mafic schist and weakly foliated metabasites. (g) View to northeast at the southernmost thrust of the Gangma Gangri thrust system (Foldout 3). Here, it places variably deformed metabasites (in black) that occur as tectonic blocks within a matrix of light-colored quartz-mica schist on top of Tertiary red beds. Some metabasites in this photo exhibit epidote-blueschist facies mineral assemblages.